Intercalibration of Boreal and Tethyan timescales: the magneto-biostratigraphy of the Middle Triassic and the latest Early Triassic from Spitsbergen (arctic Norway)

Mark W. Hounslow[1], Mengyu Hu[1], Atle Mørk[2,6], Wolfgang Weitschat[3], Jorunn Os Vigran[2,4], Vassil Karloukovski[1] & Michael J. Orchard[5]

[1] CEMP, Geography Dept., Lancaster University, Bailrigg, Lancaster LA1 4YB (m.hounslow@lancs.ac.uk).

[2] SINTEF Petroleum Research, NO-7465 Trondheim, Norway (Atle.Mork@iku.sintef.no).

[3] Geological-Palaeontological Institute and Museum, University of Hamburg, Bundesstr. 55, D-20146 Hamburg, Germany (fg6a106@geowiss.uni-hamburg.de).

[4] Mellomila 2. NO-7018 Trondheim, Norway (vigran@online.no).

[5] Geological Survey of Canada, 101-605 Robson St, Vancouver, BC, V6B 5J3, Canada (MOrchard@nrcan.gc.ca).

[6] Dept. of Geology and Mineral Resources Engineering, NTNU, Norwegian University of Sciences and Technology, NO-7491, Trondheim, Norway.

Abstract

An integrated bio-magnetostratigraphic study of the latest Early Triassic to the upper parts of the Middle Triassic, at Milne Edwardsfjellet (central Spitsbergen), allows a detailed correlation of Boreal and Tethyan biostratigraphies. The biostratigraphy consists of ammonoid and palynomorph zonations, supported by conodonts, through some 234 m of succession in two adjacent sections. The magnetostratigraphy consists of ten substantive normal-reverse polarity chrons defined by sampling at 150 stratigraphic levels. The magnetisation is carried by magnetite and an unidentified magnetic sulphide, and is difficult to fully separate, from a strong present-day like magnetisation. The bio-magnetostratigraphy from the late Olenekian (Vendomdalen Member) is supplemented by data from nearby Vikinghøgda. The early and mid Anisian has a high sedimentation rate, comprising over half the ca. 140 m thickness of the Botneheia Formation, whereas the late Anisian and lower Ladinian is condensed into about 20 m. The two latest Boreal Ladinian ammonoid zones are absent due to erosional truncation below the Tschermakfjellet Formation. Correlation to Tethyan bio-magnetostratigraphies shows the traditional base of the Boreal Anisian (base of *G. taimyrensis* Zone) precedes the base Anisian (using here definitions based on the Desli Caira section in Romania). The Boreal upper Anisian *G. rotelliforme* and *F. nevadanus* ammonoid zones correlate to most of the Tethyan Pelsonian and Illyrian substages. The base Ladinian defined in the Tethyan GSSP is closely equivalent to the traditional base of the Boreal Ladinian at the *I. oleshkoi* Zone. The latest Olenekian to early Anisian magnetic polarity timescale is refined using the Spitsbergen data.

Keywords: Magnetostratigraphy, ammonoid biostratigraphy, conodonts, boreal, Middle Triassic

Introduction

High resolution correlation and chronostratigraphy is increasingly demanded for solving problems such as understanding palaeoclimatic and faunal changes at a global scale, defining stage boundaries, basin evolution and modelling and many other purposes. Such correlations are problematic in the Mesozoic, since low latitude and high latitude faunas and floras were often very different, hence often limiting the use of biostratigraphy for global correlation. Tools of physical stratigraphy (such as magnetostratigraphy, sequence stratigraphy, cyclostratigraphy and chemostratigraphy) potentially provide local higher resolution but often need to be calibrated against conventional biostratigraphy to test their true utility. This work tests the relationship between the Boreal and Tethyan ammonoid biostratigraphies by using the pattern of reverse to normal polarity changes gained from magnetostratigraphy, as a cross-calibration tool to published bio-magnetostratigraphies for the Middle Triassic (Muttoni et al. 1998, 2000; 2004; Nawrocki & Szulc 2000). The most complete of these in low latitudes is constructed from a composite of many sections tied together by conodont and magnetostratigraphic correlations (Muttoni et al. 2000, 2004). In contrast, this work utilises a continuous succession from the latest Lower Triassic (Spathian) to the upper parts of the Middle Triassic (late Ladinian).

Lower and Middle Triassic of Svalbard

The Triassic geology of Svalbard and adjacent parts of the Barents Sea continental shelf (Fig. 1) have a regional lithostratigraphy, defined on the basis of outcrops of Triassic rocks on the Svalbard archipelago, shallow stratigraphic cores and hydrocarbon exploration wells in the surrounding seas (Mørk et al. 1999a). The Lower and Middle Triassic succession of Svalbard consists of fine-grained siliciclastics with a dominant sediment supply from the west, resulting in deposits of coastal and shallow marine sandstones and shales in western Spitsbergen, and shales and siltstones in basinal settings in central and eastern Spitsbergen, Barentsøya and Edgeøya (Figs. 1, 2). This sedimentary pattern continues southwards under the Barents Sea, with deposition of shales in basins and coarser grained clastics along the basin margins and local highs. Within eastern and central Spitsbergen the Sassendalen Group is divisible into the Vikinghøgda and Botneheia formations (Mørk et al. 1999a) which span the Lower and Middle Triassic (Fig. 1). The Lower and Middle Triassic possess sporadic Olenekian, Anisian and Ladinian ammonoid faunas, which can be closely related to richer

and more complete ammonoid faunas in NE Asia and British Columbia (Weitschat & Dagys 1989; Dagys & Weitschat 1993; Dagys & Sobolev 1995; Fig. 1). In contrast to ammonoids, the palynology from the Triassic on Svalbard and cores from the Barents Sea provides mostly continuous recovery, resulting in concurrent range zonations that have been dated by the co-occurring ammonoids (Hochuli et al., 1989; Vigran et al., 1998).

Section details

The bio-magnetostratigraphy of two sections on the southern flanks of Milne Edwardsfjellet, referred to as the MES (78.2169°N, 17.5019°E' to 78.2186°N, 15.5183°E), and ME sections (78.2169°N, 17.5025°E to 78.2183°N, 17.5169°E) are documented (Figs. 2, 3). Additional sections to the west at Milne Edwardsfjellet (MEE section) have been described by Hounslow et al. (2007a) through the uppermost part of the Botneheia Formation (Fm), into the lowest beds of the overlying Tschermakfjellet Fm; and through the entire Lower Triassic at Vikinghøgda (Fig. 2; Mørk et al. 1999b; Hounslow et al. inpress).

The region around Vendomdalen is within the NE part of the Central Tertiary Basin of southern Spitsbergen and is structurally bounded to the west by the Billefjorden Fault Zone, and to the east by the Lomfjorden- Argardbukta Fault Zone, a structural unit refereed to as the Ny Friesland Block (Fig. 2). This block shows evidence of inversion during the Early Tertiary, synchronous with folding in west Spitsbergen (Haremo & Andresen 1992).

The Vendomdalen Member (Mb) consists of silty dark grey laminated mudstone, with silty yellow-weathering diagenetic (ferroan) dolomite beds and nodules (Fig. 4). A shift from grey to dark grey mudstone takes place at the lower boundary with the underlying Lusitaniadalen Mb. Dolomitic nodules and beds, some of them septarian, are up to ~30 cm in thickness. The upper part of the member forms a pronounced dolomitic siltstone cliff approximately 5 m thick (Figs. 3a, 4a). The top of the cliff is formed by a bioturbated bed, between 0.5 and 1 m in thickness which contains abundant phosphate nodules. This bed is regarded as part of the Botneheia Fm. The overlying shales also contain abundant phosphate nodules.

The Botneheia Fm consists of bituminous shales and mudstones with occasional siltstones (forming steps in the hillside; Fig. 3b). It is divided into a lower unit of relatively soft shales, overlain by an upper unit of cliff-forming shales-the Blanknuten Mb (Figs. 3b, 5a). The middle part of the Botneheia Fm contains several carbonate cemented siltstone beds that continue

throughout the observable exposure (Fig. 3b). Phosphate is abundant both in such beds and in the interbedded shales (Fig. 5). The shales weather to papery laminations. The unit is rich in small phosphate nodules, attesting to a period of high organic productivity. The unit also has minor carbonate concretions, and layers of phosphatic and yellow-weathering dolomitic layers in the upper part of the unit. Thin limestone beds at ~100 m and upwards, are dominated by minute bivalve shells forming coquina beds with *Tasmanites* alga (Fig. 5a).

The complete Botneheia Fm appears to be exposed at Milne Edwardsfjellet, but the upper part of the formation in the ME section is disturbed by a regional décollement (Andresen et al. 1992). The uppermost 18 m of the Botneheia Fm is better exposed, without structural disturbance at the MEE section to the west, described by Hounslow et al. (2007a). The décollement formed during the Palaeocene/Eocene, synchronous with more severe folding in western Spitsbergen (Haremo & Andresen 1992).

Methods

In total 150 palaeomagnetic sample levels were collected through the succession (33 horizons were collected from the MES section, 117 from the ME section), often from concretionary calcite and dolomitic beds in the Vendomdalen Mb, and parts of the Botneheia Fm. The intervening shale lithologies in the Vendomdalen Mb were often too heavily fractured (i.e. 1-2 cm shale pieces) to collect oriented samples which could be measured. Samples from the Botneheia Fm are mostly from mudstones and shales, and a few siltstone beds lower in the formation. In both sections, bedding dips are about 3^{o} in a SE direction. The samples were predominantly oriented hand-samples, although in the harder suitable lithologies, samples were collected by a water cooled field drilling device. Samples were orientated using a dip-meter and magnetic compass.

In all 292 specimens were demagnetised. Both thermal demagnetisation and alternating demagnetisation was utilized, using either a Magnetic Measurements Ltd thermal demagnetizer or a Molspin alternating field (AF) demagnetizer. A composite demagnetisation scheme using thermal demagnetisation to 200^{o}C to 350 ^{o}C (dictated by lithology) followed by AF demagnetisation (to ~70-100 mT) was found to be most effective. Much above a critical temperature (above~ 250^{o}C) the samples often showed large changes in mineralogy (large susceptibility and intensity increases), which limited any useful

additional information obtained by thermal demagnetisation, hence AF demagnetisation was utilised above this critical temperature to better isolate the Triassic magnetisation. At most horizons at least 2 specimens were measured from each level. The specimens were measured on a CCL GM400 3-axis cryogenic magnetometer (noise level ~0.002 mA/m). ChRM directions were isolated using principle component analysis as implemented in LINEFIND (Kent et al. 1983). Use has been made of both linear trajectory fits and great circle data in defining the palaeomagnetic behaviour.

Considering the dominance of pyrite-bearing organic-rich shale and siltstone in the formations, there was expectation that magnetic sulphides (greigite, pyrrhotite) might make a significant contribution to the magnetisation, so suitable tests were performed to try and identify these. Progressive isothermal remanent magnetisation (IRM) up to 1 T, was applied to a representative sub-set of specimens, to investigate the coercivity behaviour. Thermal demagnetisation of a three component IRM was used to investigate the blocking and alteration temperature behaviour (Lowrie, 1990). Magnetisation-temperature behaviour at low temperatures (using a Princeton Measurements Ltd Magnetic Property Measurements System), were used to test for magnetite and pyrrhotite structural transitions.

Samples for palynology were collected in parallel with the magnetostratigraphy. These were preferentially collected from shale units interbedded in the sequence, and processed using standard techniques in the SINTEF laboratory. A sub-set of samples, at selected palaeomagnetic sampling horizons, were processed for conodonts at the Geological Survey of Canada (Vancouver).

Ammonoid and conodont biostratigraphy

At the base of the MES section the ammonoid *Xenoceltites subevolutus* occurs in the uppermost part of the Lusitaniadalen Mb (Fig. 4a). A parallel section a few 10's of metres to the east contains the ammonoids *Anawasatchites* sp.*, Arctoprionites nodosus, Xenoceltites subevolutus, Anasibirites* sp.*, Tellertites furcatus,* and *Pseudosageceras* sp. at the same level, indicating the latest Smithian *Anawasatchites tardus* Zone (Figs. 1, 4). A conodont collection from the 3 m level (in the Lusitaniadalen Mb; Fig. 4) comprises *Neospathodus waageni*, a Smithian index species (Sweet, 1970).

The presence of the *Bajarunia euomphala* Zone of early Spathian age is indicated by the occurrence of the zonal fossil *Bajarunia euomphala* approximately 11.2 m above the base (Fig. 4a). Above this a thin *Parasibirites grambergi* Zone (middle Spathian) is indicated by the ammonoid *Parasibirites* cf. *elegans* (Dagys & Sobolev 1995).

The major part of the Vendomdalen Member is latest Spathian corresponding to the *Keyserlingites subrobustus* Zone based on occurrences of *Keyserlingites* sp. starting from the 26 m level (Fig. 4a). In the section some 15 m below the top of the Vendomdalen Mb a diverse fauna occurs of the ammonoids *Svalbardiceras spitzbergensis, Keyserlingites subrobustus, Popovites occidentalis, Monacanthites monceros*, *Procarnites* cf. *modestus*, *Arctomeekoceras* n. sp., and *Pseudosageceras* n. sp., and the bivalve *Posidonia aranea.* A similar section a few 10's of metres to the east (visible in Fig. 3) displays the same fauna some 20 m below the top of the Vendomdalen Mb. Here, *Keyserlingites subrobustus* occurs in the cliff just below the base of the Botneheia Fm (Fig. 4a). This fauna belongs to the latest Spathian *Keyserlingites subrobustus* Zone, and *Svalbardiceras spitzbergensis* indicates the youngest sub-zone of the Siberian Olenekian (Dagys & Sobolev 1995).

Four conodont collections were recovered from the Vendomdalen Member, at 36 m, 53 m, 54.1 m, and 59.4 m. Each contains neogondolellids, some of which resemble the Siberian species *N. paragondolellaeformis* described from the latest Olenekian of Siberia (Dagys, 1984; Klets, 1998).

The macrofossil content of the ME section is relatively sparse and fossils were collected along wide exposures and laterally tied into the measured section (Fig. 5a). The first extensive dolomitic siltstone beds contain the ammonoid *Grambergia* sp. of early Anisian age (Fig. 5), without direct evidence of the earliest Anisian in the section. Nevertheless, the ammonoid *Karangatites evolutus* occurs within the lowest 1 m of the Botneheia Fm at Wallenbergfjellet (northern side, some 9.4 km to the NNE) equating with the 2nd ammonoid subzone of the *Grambergia taimyrensis* Zone, indicating the earliest Anisian is probably present in the sections in the eastern Sassendalen region. This is supported by a sample from the 21.5 m level which contains the conodonts *Chiosella timorensis* and *Neogondolella* ex gr. *regalis*, which also imply an early Anisian age (Orchard et al. 2007).

The middle part of the unit (Fig. 5) contains the ammonoids *Amphipopanoceras* c.f. *medium, Stannakhites hayesi, Anagymnotoceras varium*, *Hollandites* sp., and *Leiophyllites* n.sp. all of Middle Anisian age. Late Anisian beds are indicated by ammonoids *Frechites laqueatus*, *Aristoptychites trochleaeformis*, *Parapopanoceras malmgreni*, *Parafrechites migayi* and the bivalve *Daonella lindstroemi*. An indicator of Early Ladinian age is the ammonoids *Aristoptychites euglyphus, Tsvetkovites varius, Ussurites* sp.*,* and the bivalve *Daonella lindstroemi* (Fig. 5). A conodont collection from 91 m contains elongate representatives of the *Neogondolella constricta* group, which can most closely be assigned to *Neogondolella aldae* (sensu Orchard & Tozer, 1997) suggesting a latest Anisian to early Ladinian age (*F. chischa* Zone to *Tuchodiceras poseidon* Zone British Columbia ammonoid zones). Hence, in comparison to the early and mid Anisian, the late Anisian and early Ladinian intervals appear distinctly condensed.

No ammonoids were found in the uppermost part of the ME section, but both the bivalves *Daonella subarctica* and *Daonella degeeri* are of Late Ladinian age (Weitschat & Dagys 1989). The MEE section to the west contains the ammonoid *Indigirophyllites spetsbergensis* with *Protrachyceras* sp. and *Daonella subarctica,* 13 m below the top of the Botneheia Fm. Two conodont productive levels occur in the MEE section, one in the top 0.2 m of the Botneheia Fm, and the second 1 m into the Tschermakfjellet Fm (Hounslow et al. 2007a). Both these levels are dominated by the conodont *Neogondolella liardensis* which in British Colombia commonly occurs through the *Frankites sutherlandi* and *Trachyceras desatoyense* zones, co-occurring with *Daxatina* sp. (Orchard, 2007). The upper level also contains *Metapolygnathus polygnathiformis* and *M*. cf. *lobatus*, the former having a more limited range in these same two ammonoid zones.

Palynology

The palynology is significant for three reasons. Firstly, the other biostratigraphic and magnetostratigraphic data from the sections provides independent assessment of the age-range of relevant miospores. Secondly, by comparison to the assemblage zones constructed by Hochuli et al. (1989) and Vigran et al. (1998), and their associated ammonoid age control (Fig. 6), the palynostratigraphy allows some additional age constraints in the sections. Thirdly, the palynology provides a more continuous record of stratigraphic change through the sections, than the conodont and macrofossil data.

Like other Triassic outcrops on Svalbard, the palynofloras from the sections are not as diverse as those from cores in the Barents Sea, detailed in the discontinuous Svalis Dome cores (Fig. 6; Vigran et al. 1998). The lack of diversity is probably a reflection of outcrop weathering. Consequently, it is not possible to assign all assemblages from outcrops to the diverse Svalis assemblages, so a mix of assemblages of Hochuli et al. (1989); and Svalis assemblages are used here (Fig. 6).

Vikinghøgda Formation

The Vikinghøgda Formation is dominated by a rather monotonous flora of pollen and spores. Bisaccate pollen comprises alete indeterminate forms and taeniate forms like *Lunatisporites;* monolete pollen includes the *Pretricolpipollenites* and *Cycadopites* groups. The trilete spores are dominantly smooth forms and small cavate ones like *Densoisporites nejburgii*. The dominant plankton is represented by leiospheres, tasmanitids and *Micrhystridium*.

The single sample from the Lusitaniadalen Mb is dominated by cavate spores *Punctatisporites* spp., and other smooth triletes (Fig. 7). There are rare *Kraeuselisporites,* but little bisaccate pollen, although Fungal remains, type 1 (Hochuli et al. 1989) are common. In view of its low diversity, this association can be regarded as equivalent to Assemblage N of Hochuli et al. (1989). Spores in the richer association, at the same level at Vikinghøgda (Mørk et al., 1999b), allow correlation with assemblage Svalis-2, of Vigran et al. (1998), which in these locations occurs with ammonoids indicative of the *A. tardus* Zone.

In the lowest part of the Vendomdalen Member (8.0-12.8 m levels at Milne Edwardsfjellet, Fig. 7) indeterminate and taeniate bisaccate pollen, *Pretricolpipollenites* sp. and *Cycadopites* spp. occur together with common to dominant cavate spores (Fig. 7), features which indicate assignment of these levels to Assemblage M of Hochuli et al. (1989). The 20.5-70.2 m interval in the MES section contains dominantly bisaccates, *Cycadopites, Pretricolpipollenites* and cavate spores, with a closest resemblance (based on relative characteristics) to Assemblage L (Fig. 6). In the youngest parts of the Vendomdalen Mb (at 80.2 m) *Jerseyiaspora punctispinosa* which defines the base of the Svalis-4 assemblage (Figs. 6, 7), is associated with incoming of spores like *Retusotriletes* sp. and common *Gordonispora fossulata* (Vigran et al., 1998).

Botneheia Formation

The basal layers of the Botneheia Formation at Milne Edwardsfjellet (MES section 106.5 m) are distinguished by a poorly preserved, low diversity and non diagnostic association of palynomorphs, dominantly *Micrhystridium* spp. (Fig. 7), an association tentatively considered as equivalent to Assemblage L . The presence of *Vittatina* spp. and *Nuskoisporites* sp. (both restricted to the Permian) indicates reworking at the 108.0 m level.

The succession of samples from the Botneheia Fm in the ME section may be divided into two major intervals, both dominated by bisaccate pollen and diverse acritarchs. Between 1.7-53.0 m there are low numbers of spores, which show some diversity (Fig. 7). Between 61.0-127.6 m, spores are rare (Fig. 7).

The consistent presence between 1.7-15.3 m of *D. nejburgii* together with *Triadispora labichensis, Acanthotriletes* sp. F (Vigran et al. 1998), *Accinctisporites circumdatus, Cordaitina minor* and *Illinites chitonoides* allows assignment to assemblage Svalis-5, which is similar to Assemblage L (Hochuli et al. 1989) in its upper range (Figs. 6, 7). The interval 40.0-53.0 m contains *Conbaculatisporites hopensis, Striatella seebergensis, Jerseyiaspora punctispinosa* and *Lueckisporites junior* which allows recognition of assemblage Svalis-6. The Svalis-6 assemblage in the ME section includes forms which according to Vigran et al (1998) have their earliest appearance in late Anisian and early Ladinian assemblages at the Svalis Dome. - i.e. *Eucommiidites microgranulatus* in Svalis-7, and *Camarozonosporites laevigatus*, *Duplicisporites granulatus*, *Kuglerina meieri*, *Protodiploxypinus doubingeri*, *Schizaeoisporites worsleyi* and *Semiretisporis* sp. 1 in Svalis-8. Clearly full understanding of palynomorph ranges in the Boreal realm is incomplete, a fact that could also be interpreted from the Russian data in Mørk et al. (1992).

At 61.0 m and above, the dominance of bisaccate pollen, along with the incoming of large specimens of *Veryhachium* reflects an environmental change, which is coincident with the increased abundance of phosphate (Fig. 5a). The presence of *D. nejburgii* up to 71.2 m could be interpreted as indicating that the Svalis-6 assemblage could be extended to this level. However, these spores are considered to represent reworking. *Chasmatosporites* sp. A and *Triadispora verrucata* at the 85.5 m level are interpreted as evidence for the Svalis-7 assemblage (Fig. 7).

Between the levels 112.7-114.0 m there is an increase of pollen diversity and the earliest record of *Protodiploxypinus decus, Ovalipollis pseudoalatus* and *Staurosaccites quadrifidus* allows recognition of the Svalis-8 assemblage. A similar assemblage in the youngest part of the Botneheia Fm in the MEE section (where it co-occurs with ammonoids of the *I. tozeri* Zone; Hounslow et al. 2007a), does not contain evidence for the distinction of younger Ladinian layers, hence Assemblage I (-G) of Hochuli et al. (1989) is interpreted for the uppermost layers of the Botneheia Fm (Fig. 7).

Palaeomagnetic results and magnetic properties

Magnetic mineralogy

In the Vendomdalen Mb magnetic susceptibility is generally some 3-fold larger in the dolomitic horizons in comparison to the non-dolomitic horizons (Fig. 4b). This may be because ferroan dolomite has an appreciable larger susceptibility than most clays and calcite (Rochette et al. 1992). The Natural Remanent Magnetisation (NRM) intensities are also strongly controlled by the lithology, with the dolomitic and calcitic concretions having significantly larger values, often exceeding 1 mA/m, in comparison to the shales and siltstones which are often less than 1 mA/m (Fig. 4c). The IRM curves (Figs. 4d,e), demonstrate there is not a consistent difference in remanence mineralogy or granulometry between these lithologies, hence this lithology-related difference may be related to the better preservation of Fe-oxides in the concretionary lithologies, since it is expected that sulphide diagenesis will have destroyed most of the originally deposited Fe-oxides (Canfield & Berner 1987).

The magnetic susceptibility allows sub-division of the Botneheia Fm into three major intervals, a lower unit from 0 to 85 m with elevated and slightly variable magnetic susceptibility, a unit with generally low susceptibility from 85 to ~100 m, and an interval from ~100-130 m with values similar to those lower in the section (Fig. 5b). The lowest 2 m of the formation also have lower values. These changes are probably related to a carbonate rich interval between 85 to 100 m, and a phosphate-rich interval in the lowest 2-3 m. The diamagnetic carbonate (and phosphates), dilute the detrital material, which is likely to be responsible for the susceptibility. In the Botneheia Fm, like the underlying Vendomdalen Mb, elevated NRM intensities of samples seem to be mostly related to concretionary carbonate lithologies (Fig. 5c).

IRM acquisition curves are similar for most samples from the Vendomdalen Mb and Botneheia Fm (Figs. 4 and 5d,f), indicating near saturation by 100-200 mT, with limited acquisition above 300 mT, indicating the remanence properties are dominated by low coercivity phases (magnetite, or a magnetic sulphide).

The 3-component IRM data from both the Vendomdalen Mb and the Botneheia Fm are similar, often showing accelerated loss of remanence in all three coercivity fractions, most often starting at about 300^{o}C, with little remanence persisting above 400-450^{o}C (Fig. 8a). This seems to coincide with the start of mineralogical alteration exemplified by the increase in susceptibility during heating (Fig. 7a). This behaviour may be attributable to greigite(?) oxidation, during demagnetisation (Dekkers et al. 2000), rather than any expression of Curie or blocking temperature, since all 3 coercivity components show similar remanence loss (Fig. 8a).

The low temperature measurements on both cooling and warming cycles shows a weak magnetite Verwey transition at about 120 K and no evidence of the pyrrhotite magnetic transition at ~ 34 K (Fig. 8b; Hunt et al. 1995). The small loss of moment on crossing the magnetite Verwey transition (some 2% on cooling and 20% on warming) may be due to either its fine grain size (<~0.2 μm), oxidation of the magnetite (King & Williams 2000), or its low abundance.

In conclusion, the magnetic properties appear to be carried by both magnetite and magnetic sulphide (greigite ?), without significant discrimination of these phases in terms of coercivity differences. It seem probable the coercivities >100-200 mT may be carried by greigite, rather than ‘soft’ haematite.

Palaeomagnetic behaviour

Thermal demagnetisation above ~250-325^{o}C often induced a large increase in susceptibility, without improvement in component identification. The most reliable demagnetisation method was to clean with thermal demagnetisation to 250-350^{o}C (temperature partly dictated by lithology), prior to the heating-induced alteration, followed by AF demagnetisation up to about 80-90 mT (Fig. 9).

Specimen demagnetisation produced two magnetisation components; firstly an often steep, downwards directed, overprint magnetisation, which was sometimes removed at lower AF demagnetisation stages (<20 mT), but often persisted into the mid or later stages (40-70 mT) of AF demagnetisation (Figs. 9a, 9b). The directional mean of this overprint component is notably displaced to the south for interpreted Triassic reverse compared to normal polarity specimens (MES-normal= 004, +81, α_{95}=4.7, N=41, MES reverse= 266, +75, α_{95}=12.1, N=23; ME- normal=013, +83, α_{95}=3.3, N=86; ME- reverse=199, +78, α_{95}=5.2, N=98). Hence, the overprint component is interpreted to be a composite, predominantly a Brunhes age overprint but combined with variable amounts of a Triassic dual polarity magnetisation (Figs. 9d,c). In 26%, and 32% of specimens from the ME and MES sections respectively, this composite magnetisation direction persisted until complete demagnetisation, without any evidence of a Triassic component.

Removal of this overprint revealed the ChRM component interpreted as a dual polarity NE and SW directed Triassic magnetisation (Figs. 9c,f). This was most often isolated above about the 40 mT AF demagnetisation stage, and was predominantly isolated through the origin, although imposed spurious instrument-derived magnetisation often hindered origin line fits (Fig. 9c). Some 28% and 23% of specimens from the MES and ME sections respectively, had suitable linear trajectory line fits (i.e. here termed S-type data). The mean directions for the ChRM line fits for ME section pass the reversal test (McFadden & McElhinney 1990; Table 1). No reverse polarity samples with S-type data were extracted from the MES section (Table 1; Fig. 10a). Some 40% and 51% of specimens from the MES and ME sections respectively, displayed great circle trends of varying arc length towards interpreted Triassic reverse and normal polarity directions (here referred to as T-type demagnetization behaviour; Figs. 9a,d,e). These great circle paths were used with the line-fits to determine combined mean directions (McFadden & McElhinney 1988). These combined mean directions pass the reversal test only for the ME section (Table 1). The reversal test on the specimen data from the MES section, fails the reversal test. There is no polarity bias in the data from sampled concretion-levels (Fig. 10a,b), although on average samples from calcite concretions posses poorer palaeomagnetic behaviour than those from dolomite concretions.

The great-circle combined means are significantly steeper than the ChRM line-fit only data

(Table 1). We consider it possible that the great circle means may be unduly biased by directional contamination in the great circle data, from the Brunhes age overprint. Hence, ChRM line-fit data probably provide the best estimates of the mean Triassic magnetic field direction for the sample set. However, in terms of comparison to the Baltica apparent polar wander path (APWP), only the combined mean for the ME-section, falls off the 95% confidence swath (Fig. 11). The ChRM line-fit means fall over the 95% confidence swath of the Baltica APWP (Fig. 11), with general westwards displacement of the means from the oldest (late Olenekian, MES section data) to the youngest (late Ladinian, MEE section data) in the Botneheia Fm (Fig. 11).

Magnetostratigraphic Results

The line-fit ChRM directions from Milne Edwardsfjellet were converted to virtual geomagnetic pole (VGP) latitude using the line-fit mean directions from each respective section (Table 1, Fig. 10c). For those specimens that had no line-fit, the point on their great circle trend nearest the mean was used for calculating the VGP latitude (Fig. 10c). All specimens were also assigned a 'polarity quality' (Fig. 10b) based on the quality of demagnetisation behaviour and, if from T-class specimens, the length and end point position of the great circle trend (similar to that used by Ogg & Steiner 1991; Hounslow et al. 2007a). One specimen of good-quality polarity (i.e. S-Type) was sufficient to define the horizon polarity, whereas with specimens of poorer quality at least two were needed (Fig. 10d). Four horizons (one from the MES and three from ME section) failed to yield any specimens which could reliably be used to determine magnetic polarity (Fig. 10d).

The resulting magnetic polarity changes through the two sections combined, has resulted in a complex pattern of polarity changes (Fig. 10d). These have been numbered into ten N-R couplets from the base of the MES section. The pattern of polarity changes is broken by substantive sampling gaps in the Vendomdalen Mb, whereas the more complete sampling through the Botneheia Fm demonstrates normal polarity dominates the lower 70 m of the formation, whereas reverse polarity dominates from this level upwards (Fig. 10d).

Discussion

The palaeomagnetic behaviour of the samples from the Vendomdalen Mb at Milne Edwardsfjellet is not significantly different from that at Vikinghøgda described by Hounslow et al. (inpress), in that extraction of reverse polarity line-fits from the demagnetisation data has proven problematic. This is probably due to the nature of the magnetisation carrier in the

Vendomdalen Mb (and also the Botneheia Fm) which appears to be a mixed magnetite-magnetic sulphide mineralogy. Presumably, if the magnetic sulphide is early diagenetic in origin, the Triassic magnetisation is probably carried by both the magnetic sulphide and magnetite.

Comparison of the bio-magnetostratigraphy in the Vendomdalen Mb between Milne Edwardsfjellet and Vikinghøgda (Hounslow et al. inpress) demonstrates differences in the pattern of polarity changes, due in part to large changes in sedimentation rate (Fig. 12). Some of these differences are compounded by the substantial sampling gaps. The reverse magnetozone MF1n.2r appears to be the equivalent of V8n.1r at Vikinghøgda, since both are immediately younger than the occurrence of *B. euomphala* in the sections. The mid-part of the Vendomdalen Mb is better characterised at Milne Edwardsfjellet, than that at Vikinghøgda, where substantial sampling gaps occur, indicating the early parts of the *K. subrobustus* Zone are of mixed polarity (Fig. 12).

The upper most part of the Vendomdalen Mb and lowest Botneheia Fm at Milne Edwardsfjellet is a dominantly reversed polarity interval, whereas this same interval is normal polarity at Vikinghøgda (Fig. 12). This suggests there is a substantial hiatus near the Vendomdalen-Botneheia boundary at Vikinghøgda, without representation of the equivalent of the MF2r or MF3 magnetozones (Fig. 12). The postulated hiatus does not violate the occurrence of *Svalbardiceras spitzbergensis*, which occurs within the upper part of magnetozone MF2n, and an equivalent interval at Vikinghøgda (Fig. 12). There is clear evidence of erosion of Permian deposits, by the reworked palynomorphs *Vittatina* sp. and *Nuskoisporites* sp. some 2.5 m above the base of the Botneheia Formation in the MES section- it seems probable that this level may represent the correlative disconformity at Milne Edwardsfjellet. The most likely correlative level between Vikinghøgda and Milne Edwardsfjellet in the base of the Botneheia Fm, is the *Rhizocorallium*-bearing siltstone some 10 m above the base of the Botneheia Fm at Vikinghøgda (Mørk et al. 1999b; Hounslow et al. inpress) which is the equivalent of the *Rhizocorallium*-bearing siltstone bed at the 30 m level in the ME section (Figs. 5, 12). These substantial magnetostratigraphic differences at the Vendomdalen-Botneheia boundary may be due to the fact that Vikinghøgda is close to the western side of the Ny Friesland Block (Fig. 2), and therefore may be more likely to have experienced minor Triassic uplift and erosion, associated with the Billefjorden basement

fault complex.

Middle Triassic magnetostratigraphy tied to Tethyan and Boreal biostratigraphy

The distinctive feature of the lower part of the Botneheia Fm is the dominance of normal polarity through magnetozones MF4n to MF7n. The Boreal ammonoids indicate an early to mid Anisian age for this interval. This appears to correspond to the dominantly normal polarity interval (MT1n to MT4n) from near the base of the Anisian to the early Pelsonian in Tethyan successions (Fig. 12). Currently, a decision on the base Anisian GSSP has not been formally ratified, but the Desli Caira candidate section has been proposed, using as the prime marker, either FAD the conodont *Chiosella timorensis* (Grãdinaru et al. 2007), or the base of magnetozone MT1n (Hounslow et al. 2007b). Using the magnetostratigraphic correlations either of these levels equates to within the lowest part of the Boreal Anisian (just above the base of the *Grambergia taimyrensis* Zone, Figs. 1, 12), following the earliest *Karangatites* sp. in the Boreal realm (Fig. 13). Correlation to the Polish Middle Triassic magnetostratigraphic data of Nawrocki & Szulc (2000) at this level is not directly constrained by any useful shared biostratigraphy, but the thicker and more complete succession through the central German Basin at this level (Szurlies 2007) shows a clear relationship to the Tethyan composite (Fig. 12). This is supported by an array of conodont and ammonite faunas in the mid and late Anisian parts of the Muschelkalk (Nawrocki & Szulc 2000; Szurlies 2007).

As a result of the high relative sedimentation rate in the lower part of the Botneheia Fm (in the ME section) the lowest Anisian reverse magnetozones (i.e. MF4n.1r, MF4r, MF5r) are much expanded compared to both the Tethyan composite and that in the Polish-German Basin (Fig. 12). The correlations proposed in Fig. 12 are supported by the occurrence of *Cs. timorensis*, which ranges up through the MT3n magnetozone at the Kçira and Desli Caira sections (Muttoni et al. 1996; Gradinaru et al. 2007; Fig. 13).

Magnetozone MF5r appears to equate to CG11r and interval S1r-S3n.1r in the Polish and German sections (Fig. 12), and also a similarly-placed reverse magnetozone in the upper Guandao section in China (Orchard et al. 2007; Hounslow et al. 2007b). The two single-horizon normal magnetozones within MF5r, appear to be confirmed by the occurrence of two normal magnetozones at the correlated level in the Upper Silesia sections (i.e. S2n and

S3n.1n; Fig. 12). The reverse magnetozone MF6r appears to be the equivalent to magnetozone S3r in the Polish Upper Silesia composite, which may also equate to a reverse magnetozone in both the lower and upper Guandao sections (Hounslow et al. 2007b; Fig. 12).

Above magnetozone MF7n is a dominantly reverse polarity interval (MF7r to MF9r). The most important constraint which allows correlation to the Tethyan sections is the base of the Ladinian GSSP at Bagolino, which is defined on the first occurrence of the genus *Eoprotrachyceras* (Brack et al. 2005). This level can be confidently correlated to the *Eoprotrachyceras matutinium* Zone (formerly *E. aspersum* Zone; Orchard & Tozer 1997) of British Columbia, bearing the first representatives of the ammonoids Trachyceratidae (Dagys & Konstantinov 1995; Brack et al. 2005). In British Columbia the immediately younger *Tuchodiceras poseidon* Zone (formally *Progonoceras poseidon* Zone; Orchard & Tozer 1997) contains *Arctoptychites* and forms related to *Tsvetkovites constantis*, allowing correlation to the *Tsvetkovites constantis* Zone of N.E. Asia and the ammonite fauna of the Svalbard *T. varius* Zone (Fig. 1; Dagys & Weischat 1993; Dagys & Konstantinov 1995). Together these indicate the base of the Ladinian is within the lower part of magnetozone MF8r (Figs. 11, 12), and the magnetozone MF9n, which contains the *T. varius* Zone fauna, is the equivalent of Tethyan magnetozone MT9n (Fig. 12). On the assumption that there is no hiatus in the ME section between MF7r and MF8r, the most probable correlation to the Tethyan sections indicates MF8n is the equivalent of MT7n, and MF7r.3n is the equivalent of MT6n (Fig. 12). The conodont *Neogondolella aldae* is a probable synonym of *N. cornuta*, which has been commonly identified in the Tethyan sections and there ranges between MT5r and the top of MT7n (Fig. 13). This relationship generally confirms the magnetostratigraphic relationships proposed. However, other alternative correlations at this level are possible, if a sequence boundary (and potential hiatus ?) are hypothesised at this level, based on comparison to the Barents Sea, where a prominent sequence boundary characterises the boundary between the Steinkobbe and Snadd formations, close to the boundary between the Svalis-7 and Svalis-8 palynozones (Vigran et al. 1998).

At least one normal magnetozone (i.e. MT5n) occurs within the dominantly reverse interval MT4r to MT5r, having been detected in the Polish Muschelkalk (magnetozone S5n in the Upper Silesia composite and the probable equivalent in the Nietulisko section; Fig. 12).

Sections at Granitivo and Nederlysaj in Bulgaria and Albania also display short duration normal magnetozones at this level (Muttoni et al. 2000). Hounslow and McIntosh (2003) have also detected possibly two short duration normal magnetozones at about this level. One or other of the putative normal magnetozones in the MF7r magnetozone may represent these intervals in the Milne Edwardsfjellet section.

At Milne Edwardsfjellet, the succession above MF9n is complicated by the decollément, and it is not certain how much of the section has been removed or repeated. Nevertheless, the continuous undisturbed MEE section through the upper-most part of the Botneheia Fm, indicates dominantly normal magnetic polarity to the top of the formation. This is supplemented by the upper-most undisturbed part across the Botneheia-Tschermakfjellet boundary in the ME section, which shows one horizon of reverse polarity (Figs. 10d & 12). We interpret the data from the overlapping ME and MEE sections as indicating one normal magnetozone (MF10n), with evidence of the overlying magnetozone MF10r from the single horizon highest in the Botneheia Fm at the ME section. Following on from the lower part of the section, would therefore suggest that MF9r is the equivalent of the combined MT9r and MT10, and MF10n is the correlative of part or all of MT11 (or MT11 to MT12n). The available biostratigraphic correlations seem to confirm this. Based on similarities and co-occurrences of ammonoids between British Columbia- NE Asia- Svalbard and the Alps, Dagys & Konstantinov (1995) suggest the Svalbard *Indigirites tozeri* Zone is approximately equivalent to the mid-parts of the *Protrachyceras archelaus* Zone of the Alps (Gredleri and Archelaus Zones combined in Fig. 12). The fact that the conodont *N. liardensis* occurs in the top-most part of the Botneheia Fm (in the MEE section), would suggest that the succession extends into beds equivalent to the *Frankites sutherlandi* Zone of British Columbia, which is equivalent to the *Nathorstites mcconnelli* Zone in NE Asia (Dagys & Konstantinov, 1995; Figs. 1 and 13).

Palynostratigraphy comparisons

In combination with the palynology from the Spitsbergen sections, our data also provides additional detail on the age constraints of the palynological assemblage zones of Vigran et al. (1998). The ammonoid-derived ages of the Svalis Dome assemblages are generally similar to those indicated here, except for the Svalis-5 assemblage, which extend downwards into the very latest parts of the Olenekian. The data from the Svalis Dome cores are consistent with this, since the well-defined Svalis-4 to Svalis-5 boundary occurs in a 10 m

interval, barren of ammonoids, between underlying occurrences of *Keyserlingites* sp. and overlying *Grambergia* sp. (Vigran et al. 1998).

The Svalis-8 assemblage may extend downwards into the latest Anisian, although the condensed sedimentation and wide sample spacing over this interval, makes this conclusion less clear. Comparison of the Boreal palynological assemblages to well-dated (i.e. using conodonts and ammonoids) in lower latitudes is problematic because of the few taxa in common (e.g. *Jerseyiaspora punctispinosa*, *Kuglerina meieri*, *Dyupetalum vicentinence*, *Cyclotriletes triassicus*, *Aratisporites tenuispinosa*), and those which are shared, being sporadically present (cf. Vigran et al. 1998; Kustatscher et al. 2006). Perhaps the simplest comparison is the Svalis-8 assemblages with the increase in *Ovalipollis* sp. (in the Svalis-8 assemblage; *O. pseudoalatus*) which characterise the transition into the *E. curionii* Zone in the Alps (Hochuli & Roghi 2002), which defines the base of the Ladinian (Brack et al. 2005; Fig. 13). The equivalence of these major palynological changes provides additional support for the placement of the base of the Ladinian in the ME section indicated in Figures 12 and 13.

Conclusions

1) The succession at Milne Edwardsfjellet provides a thick (~110 m) and comparatively complete succession through the latest Spathian into the mid Anisian, whereas the late Anisian to Ladinian is comparatively condensed into about 70 m, with the latest Ladinian absent (i.e. younger than approximately the *Nathorstites mclearni* Zone).
2) The succession preserves a Triassic magnetostratigraphy, carried by magnetite and a magnetic sulphide, which is in part overprinted with a Brunhes-like magnetisation.
3) The mean magnetisation directions demonstrate the close affinity to the early Mesozoic apparent polar wander path of Baltica, demonstrating that the magnetisation directions are primary.
4) The high sedimentation rate through the latest Olenekian into the early Anisian allows refinement of the magnetic polarity timescale over this interval.
5) Discontinuous ammonoid and conodont recovery levels, assisted by palynostratigraphy provide clear constraints for magnetostratigraphic correlation to bio-magnetostratigraphies determined from lower latitudes. Age refinements of the Barents Sea regional palynostratigraphic zonation also result from this integrated

stratigraphy.

6) The base of the Anisian, informally defined in the Desli Caira section in Romania maps onto an interval in the Boreal stratigraphy between the upper part of MF3r and mid parts of MF4n.1r, equating to an interval within the Siberian *Grambergia taimyrensis* Zone.
7) The base of the Ladinian in the Bagolino GSSP (Brack et al. 2005) maps closely onto the traditional base Ladinian (i.e. base of *Intornites oleshkoi* Zone) used in the Boreal realm.

Acknowledgements

Technical staff at IKU/SINTEF Petroleum Research and Lancaster (Simon Chew) helped with illustrations. The project was supported by Saga Petroleum ASA, Norsk Hydro ASA and Deminex. Morten Bergan and Rob Hawkins assisted in the field with palaeomagnetic sample collection. Valuable comments from Jerzy Nawrocki and Jim Ogg improved the manuscript. This is a contribution to IGCP project 467. The magnetostratigraphic data is archived in the MaGIC database.

References

Andresen A., Haremo P., Swensson E. & Bergh S.G. 1992. Structural geology around the southern termination of the Lomfjorden Fault Complex, Agardhdalen, east Spitsbergen. *Norsk Geologisk Tidsskrift*, *72*, 83-91.

Brack P., Riener H., Nicora A. & Mundil R. 2005. The global boundary stratotype and point (GSSP) of the Ladinian Stage (Middle Triassic) at Bagolino (Southern Alps, Northern Italy) and its implication for the Triassic timescale. *Episodes 28*, 233-244.

Canfield D.E & Berner, R.A. 1987. Dissolution and pyritisation of magnetite in anoxic marine sediments. *Geochimica et Cosmochimica Acta 51*, 645-659.

Dagys, A.A. 1984. Early Triassic conodonts of northern central Siberia. *Transactions Institute of geology and geophysics, Academy of Sciences, USSR, Siberian branch 554*, 1-69. (in Russian)

Dagys A.S. & Weitschat W. 1993. Correlation of the Boreal Triassic. *Mitteilungen Geologisch-Paläontologisches Institut Universität Hamburg 75*, 249-256.

Dagys A.S. & Konstantinov A.G. 1995. New zonation scheme of the Ladinian Stage for Northeastern Asia. *Stratigraphy and Geological Correlation 3*, 121-127.

Dagys A.S. & Sobolev E.S. 1995. Parastratotype of the Olenekian Stage (Lower Triassic). *Albertiana 16*, 8-16.

Dallmann W.K. (ed.) 1999. *Lithostratigraphic lexicon of Svalbard. Review and recommendations for nomenclature use. Upper Palaeozoic to Quaternary bedrock*. Tromsø: Norsk Polarinstitutt.

Dekkers M.J., Passier H.F. & Schoonen M.A.A. 2000. Magnetic properties of hydrothermally synthesized greigite (Fe_3S_4)-II. High and low-temperature characteristics. *Geophysical Journal International 141*, 809-819.

Grădinaru E., Orchard M.J.. Nicora A., Gallet Y., Besse J., Krystyn L., Sobolev E.S., Atudorei, N-V., Ivanova D. 2007. The global boundary stratotype section and point (GSSP) for the base of the Anisian: Dęsli Caira Hill, North Dobregeo, Romania. *Albertiana* 36, 44-57.

Haremo P. & Andresen A. 1992: Tertiary décollement thrusting and inversion structures along Billefjorden and Lomfjorden Fault Zones, east central Spitsbergen. In R.M. Larsen, H. Brekke, B.T. Larsen & E. Talleraas (eds.): *Structural and tectonic modelling and its application to petroleum geology*, Pp. 481-494. Norwegian Petroleum Society, Special Publication, 1, Amsterdam: Elsevier.

Hochuli P.A., Colin J.P. & Vigran J.O. 1989: Triassic biostratigraphy of the Barents Sea area. In J.D. Collinson (ed.): *Correlation in Hydrocarbon Exploration*. Pp131-153. Norwegian Petroleum Society (NPF), London: Graham & Trotman Ltd.

Hochuli P.A. & Roghi, G. 2002. A palynological review of the Anisian-Ladinian boundary- new results from the Seceda section (Dolomites, Northern Italy). STS/IGCP 467 conference guide, Veszprem, Hungary, 5-8th September, 2002. Geological Institute of Hungary, Pp 29-30.

Hounslow M.W. & McIntosh G. 2003. Magnetostratigraphy of the Sherwood Sandstone Group (Lower and Middle Triassic), south Devon, UK: detailed correlation of the marine and non-marine Anisian. *Palaeogeography, Palaeoclimatology, Palaeoecology 193*, 325-348.

Hounslow M.W., Hu M., Mørk A., Vigran J.O., Weitschat W. & Orchard M.J. 2007a. Magneto-biostratigraphy of the lower part of the Kapp Toscana Group (Carnian), Vendomdalen, central Spitsbergen, arctic Norway. *Journal of the Geological Society London 164*, 581-597

Hounslow, M.W. Szurlies, M., Muttoni, G., Nawrocki, J. 2007b. The magnetostratigraphy of the Olenekian-Anisian boundary and a proposal to define the base of the Anisian using a magnetozone datum. *Albertiana* 36, 62-67.

Hounslow M.W., Peters C., Mørk A., Weitschat W. & Vigran J.O. inpress. Bio-magnetostratigraphy of the Vikinghøgda Formation, Svalbard (arctic Norway) and the geomagnetic polarity timescale for the Lower Triassic. *Geological Society of America Bulletin*.

Hunt C.P., Moskowitz B.M. & Banerjee S.K. 1995: The magnetic properties of rocks and minerals. In Ahrens T, J. (ed.): *Global Earth Physics- Handbook of physical constants*. Pp. 189-204. Boston: American Geophysical Union.

Kent J.T., Briden J.C. & Mardia K.V. 1983. Linear and planar structure in ordered multivariate data as applied to progressive demagnetisation of palaeomagnetic remanence. *Geophysics Journal Royal Astronomical Society 81*, 75-87.

King, J.G. & Williams W. 2000. Low temperature magnetic properties of magnetite. *Journal of Geophysical Research 105*, 16427-16436.

Klets T.V. 1998. New species of conodonts from the Lower Triassic of the Kolyma basin. *News of paleontology and stratigraphy, issue 1, Supplement to Geologiya I Geofizika 39*, 113-121 (in Russian).

Kustatscher E., Manfrin S., Mietto P., Posenato R. & Roghi G. 2006. New biostratigraphic data on Anisian (Middle Triassic) palynomorphs from the Dolomites. *Review of Palaeobotany and Palynology, 140*, 79-90.

Lehrmann, D.J, Ramezani J., Bowring, S.A., Martin M.W., Montgomery, P., Enos P., Payne J.L. , Orchard M.J. Hongmei W., & Jiayong W. 2007. Timing of recovery from the end-Permian extinction: Geochronologic and biostratigraphic constraints from south China. *Geology 34*, 1053-1056.

Lowrie W. 1990. Identification of ferromagnetic minerals in a rock by coercivity and unblocking temperature profiles. *Geophysical Research Letters, 17*, 159-162.

McFadden P.L. & McElhinney M.W. 1988. The combined analysis of remagnetisation circles and direct observations in palaeomagnetism. *Earth and Planetary Science Letters 87*, 161-172.

McFadden P.L. & McElhinny M.W. 1990. Classification of the reversal test in palaeomagnetism. *Geophysical Journal International 103*, 725-729.

Muttoni G., Kent D.V., Meço S., Nicora A., Gaetani M., Balini M., Germani D. & Rettori R. 1996. Magnetobiostratigraphy of the Spathian to Anisian (Lower to Middle Triassic) Kçira section, Albania. *Geophysical Journal International 127*, 503-514.

Muttoni G., Kent D.V., Meço S., Balini M., Nicora A., Rettori R., Gaetani M. & Krystyn L. 1998. Towards a better definition of the Middle Triassic magnetostratigraphy and biostratigraphy in the Tethyan realm. *Earth and Planetary Science Letters, 164*, 285-302.

Muttoni G., Gaetani M., Budurov K., Zagorchev I., Trifonova E., Ivanova D., Petrunova L. & Lowrie W. 2000. Middle Triassic palaeomagnetic data from northern Bulgaria: constraints on Tethyan magnetostratigraphy and palaeogeography. *Palaeogeography Palaeoclimatology Palaeoecology 160*, 223-237.

Muttoni G., Nicora A., M., Brack P. & Kent D.V. 2004. Integrated Anisian–Ladinian boundary chronology. *Palaeogeography, Palaeoclimatology, Palaeoecology 208*, 85– 102.

Mørk A., Vigran J.O., Korchinskaya M.V., Pchelina T.M., Fefilova L.A., Vavilov M.N. & Weitschat W. 1992: Triassic rocks in Svalbard, the Arctic Soviet islands and the Barents Shelf: bearing on their correlations. In T.O. Vorren et al. (eds.): *Arctic Geology and Petroleum Potential*. Pp. 457-479. Norwegian Petroleum Society, Special Publication No. 2, Amsterdam: Elsevier.

Mørk A., Dallmann W.K., Dypvik H., Johannessen E.P., Larssen G.B., Nagy J., Nøttvedt A., Olaussen S., Pchelina T.M. & Worsley D. 1999a: Mesozoic lithostratigraphy. In W.K., Dallmann (ed.): *Lithostratigraphic lexicon of Svalbard. Review and recommendations for nomenclature use. Upper Palaeozoic to Quaternary bedrock*. Pp. 127-214.Tromsø: Norsk Polarinstitutt.

Mørk A., Elvebakk G., Forsberg A.W, Hounslow M.W., Nakrem H.A., Vigran J.O. & Weitschat W. 1999b. The type section of the Vikinghøgda Formation: a new Lower Triassic unit in central and eastern Svalbard. *Polar Research 18*, 51-82.

Nawrocki J. & Szulc J. 2000. The Middle Triassic magnetostratigraphy from the Peri-Tethys basin in Poland. *Earth Planetary Science Letters 182*, 77–92.

Ogg J.G. & Steiner M.B. 1991. Early Triassic polarity time-scale: integration of magnetostratigraphy, ammonite zonation and sequence stratigraphy from stratotype sections (Canadian Arctic Archipelago). *Earth Planetary Science Letters 107*, 69-89.

Orchard M.J., & Tozer E.T. 1997. Triassic conodont biochronology, its calibration with the ammonoid standard and a biostratigraphic summary for the western Canada sedimentary basin. *Bulletin Canadian Petroleum Geology 45*, 675-692.

Orchard, M.J. 2007. New conodonts and zonation, Ladinian-Carnian boundary beds, British Columbia, Canada. *New Mexico Museum of Natural History and Science Bulletin 41*. 321-330.

Orchard, M.J., Gradinaru. E., & Nicora, A. 2007. A summary of the conodont succession around the Olenekian-Anisian boundary at Deşli Caira, Dobrogea, Romania. *New Mexico Museum of Natural History and Science Bulletin 41*. 341-346.

Rochette P., Jackson M. & Auboug C. 1992. Rock magnetism and the interpretation of anisotropy of magnetic susceptibility. *Reviews in Geophysics, 30*, 209-226.

Sweet, W.C., 1970: Uppermost Permian and Lower Triassic conodonts of the Salt Range and Trans-Indus Ranges - West Pakistan. In Kummel, B., Teichert, C. (eds.), *Stratigraphic Boundary Problems: Permian and Triassic of West Pakistan*. Pp. 207-275. University of Kansas, Special Publications 4.

Szurlies, M. 1007. Latest Permian to Middle Triassic cyclo-magnetostratigraphy from the Central European Basin, Germany: Implications for the geomagnetic polarity timescale. *Earth and Planetary Science Letters* 261, 602–619.

Torsvik T.H. & Cocks L.R.M. 2005. Norway in space and time: A centennial cavalcade. *Norwegian Journal of Geology 85*, 73-86.

Tozer E.T. 1994. Canadian Triassic ammonoid faunas. *Bulletin Geological Survey Canada*, 467, 663pp.

Vigran J.O., Mangerud G., Mørk A., Bugge T. & Weitschat W. 1998. Biostratigraphy and sequence stratigraphy of the Lower and Middle Triassic deposits from the Svalis Dome, Central Barents Sea, Norway. *Palynology 22*, 89-141.

Vigran J.O., Mørk A. & Worsley D unpubl ms. Palynology and geology of the Triassic succession of Svalbard. *NGU Bulletin*.

Weitschat W. & Dagys A.S. 1989. Triassic biostratigraphy of Svalbard and a comparison with NE-Siberia. *Mitteilungen Geologisch-Paläontologisches Institut Universität Hamburg 68*, 179-213.

Figure Captions

Fig. 1. Lithostratigraphy and ammonoid biostratigraphy of Svalbard and other key Boreal areas Ammonoid zones from Dagys & Weitschat (1993), Tozer (1994) and Dagys & Sobolev (1995).

Fig. 2. Location map of Deltadalen in central Spitsbergen, and a simplified geology of southern Svalbard (modified from Dallmann, 1999). Separate legends for main map and inset. BFZ= Billefjorden fault Zone, LAFZ= Lomfjorden- Argardbukta Fault zone. Inset shows the location of the sections at Milne Edwardsfjellet (MES, ME sections) and the MEE section described by Hounslow et al. (2007a).

Fig. 3. a) The upper-most part of the MES section (Vendomdalen Mb). The top-most part of the ledge in the middle distance is the base of the Botneheia Fm overlying the top of the Vendomdalen Mb. The more easily weathered softer shales in the base of the Botneheia Fm overly this. Scale relates to Fig. 4a. b) The ME section, with photo taken from near the base of the Botneheia Fm. The darker, steep-cliff forming units are the Blanknuten Mb, near the top of the formation.

Fig. 4. MES section summary through the Vendomdalen Mb. a) lithological log, biostratigraphy and palynostratigraphic sampling levels. b), c) Specimen magnetic properties, and d), e) representative isothermal remanent magnetisation curves. Positions of samples (MES code) figured and discussed in text adjacent to the magnetic susceptibility column (b). Fauna codes: X.s= *Xenoceltites subevolutus*; B.e.= *Bajarunia euomphala*; P.e.=*Parasibirites* cf. *elegans*; K.= *Keyserlingites* sp.; K.s. *Keyserlingites subrobustus*; P.m=*Posidonia mimer*; S.s= *Svalbardiceras spitzbergensis*; P.o= *Popovites occidentalis.* L. Mb= Lusitaniadalen Mb.

Fig. 5. ME section summary of the Botneheia Fm. a) lithological log, biostratigraphy and palynostratigraphic sampling levels. b), c) Specimen magnetic properties, and d) to e) representative isothermal remanent magnetisation curves. Positions of samples (ME code) figured and discussed in text adjacent to the magnetic susceptibility column (b). Fauna codes: A.e= *Aristoptychites euglyphus*; A.v.= *Anagymnotoceras varium*; A.m= *Amphipopanoceras* c.f. *medium;*S.h= *Stannkhites hayesi*; P.v= *Parapopanoceras malmgreni*; P.t.= *Aristoptychites trochleaeformis*; F.l= *Frechites laquatus;* T.v= *Tsvetkovites varius;* P.m= *Parafrechites migayi;* D.l= *Daonella lindstroemi*. Key to lithological log in Fig. 4.

Fig. 6. Key miospore ranges that define the palynostratigraphy in the zonations of Hochuli et al. (1989) from Svalbard and the Barents Sea and Vigran et al. (1998) for the Svalis Dome cores. The associated ammonoids, which date the zonations are those indicated by Hochuli et al. (1989) and Vigran et al. (1998). The miospore species and genera indicated in bold are key markers used in defining the assemblage zones. Triassic stage assignment for the Svalis Dome zonation is in part based on this work.

Fig. 7. Palynology of the Milne Edwardsfjellet sections (modified from Vigran et al., unpubl. ms). See Figs 4 and 5 for location of samples. Miospores indicated in bold are of stratigraphic significance for correlation. *Striatoabieites* and *Triadispora* taxa have been presented as groups. L.= Lusitaniadalen Mb; B.F. Botneheia Fm. Stage assignment based on this work.

Fig. 8. a) Thermal demagnetisation of a three component IRM for representative samples from the Vendomdalen Mb and the Botneheia Fm. Specimen stratigraphic location shown in Figs. 4 and 5. b) Low temperature remanence measurements on two specimens, showing zero field cooling of a room temperature 300 mT IRM, and warming of a 2.5 T IRM applied at 10 K (normalised to moment at 10 K). Specimen stratigraphic location shown in Fig. 5.

Fig. 9. Representative specimen demagnetisation data, specimen location on Figs. 4 and 5. Detail of the Zijderveld plots for a), b) and d) is shown on the right of the stereonet in each case. a) MES308A (14.3 m; Limestone nodule), demonstrates great circle-type behaviour (demagnetisation class T2) trending towards reverse polarity, removing a NW directed (323^{o}, 62^{o}) composite component. Fitted great circle between 200^{o}C and origin, with pole at 101^{o}, +19^{o}. b) MES322B (63.2 m, dolomite nodule), illustrating removal of a steep present-day like direction (347^{o}, 83^{o}, from 300^{o}C to 60 mT), and isolation of an interpreted Triassic normal polarity direction (016^{o}, 66^{o}) from 70 mT to the origin (demagnetisation class S3). c) MES334C (105.8 m, phosphatic siltstone) shows the isolation of an interpreted Triassic normal polarity between 50 and 90 mT (032^{o}, 56^{o}, demagnetisation class S2), after removal of a slightly steeper lower stability component (315^{o}, 67^{o}). d) ME16A (24.5 m, pale grey siltstone), demonstrates great circle behaviour (pole at 090^{o}, 2^{o}, demagnetisation class T1) towards an interpreted reverse polarity direction, up to 100 mT demagnetisation. e) ME53A (62.7 m, cemented shale) shows great circle behaviour (pole at 059^{o}, 18^{o}, demagnetisation class T2) towards an interpreted reverse polarity . The composite low stability component has a line fit direction of 194^{o}, 67^{o} between 200^{o}C and 100 mT. F) ME72C (84.5 m, paper shale), shows isolation of a line fit ChRM direction (200^{o}, -60^{o}, demagnetisation class S1) between 10 and 70 mT demagnetisation. [...] is the scale between ticks on the Zijderveld plot.

Fig. 10. Magnetostratigraphic data of the specimens. a) Demagnetisation behaviour showing categorisation into good (S1) and poor (S3) linear line-fits; great circle fits range from good (T1) to poor, and specimens with no (P/X) Triassic magnetisation (see text for details). Squares on right-hand-side of column indicate sample levels from dolomite (filled) and calcite (unfilled) concretions. b) The interpreted specimen polarity quality, with those in the mid-grey column not assigned a polarity (??= poorest quality for reverse and normal). c) The virtual geomagnetic pole latitude (VGP), with filled symbols for those specimens possessing an S-class ChRM, and unfilled symbols the VGP latitude for specimens with T-class great-circle behaviour. d) Horizon polarity: white= reversed polarity, black =normal polarity, grey= uncertain; half bar-width indicates a single useful specimen from this horizon.

Fig. 11. Mean virtual geomagnetic poles with respect to the apparent polar wander path (APWP) for Baltica. 95% confidence swath around the mean APWP (from Torsvik and Cocks, 2005) indicated with hash ornamentation. Poles (filled circles) marked in 10 My increments, using the timescale in the palaeomagnetic database. Line-fit only means indicated with grey 95% confidence cones, non-filled are combined great circle and line-fit means in Table 1. Data for the MEE section, in the upper-most part of the Botneheia Fm, from Hounslow et al. (2007a).

Fig. 12. Other selected late Olenekian and Middle Triassic bio-magnetostratigraphies and probable correlations to the Central Spitsbergen sections. Vikinghøgda data from Hounslow et al. (in press). Tethys data compiled from Muttoni et al. (2000; 2004), Grădinaru et al. (2007), Lehrmann et al. 2007; Orchard et al. 2007) and discussion in Hounslow et al. (2007b). Magnetozones in the Alps column numbered from the base to ease description in the text. Polish data from Nawrocki & Szulc (2000), German composite from Szurlies (2007) with minor additional details and Polish-German correlations from Hounslow et al. (2007b). MEE section data from Hounslow et al. (2007a). S.s= *Svalbardiceras spitzbergensis*. Olenekian-Anisian boundary interval is based on the Dęsli Caira section in Romania, with its two proposed boundary criteria (Grădinaru et al. 2007; Hounslow et al. 2007b), neither of which has been formally ratified.

Fig. 13. Composite global Middle Triassic magnetostratigraphy and its correlation to the Boreal (NE Asia) ammonoid timescale and the composite Tethyan magneto-biostratigraphy (Peri-Tethys and Tehtys sections in Fig. 12). Conodont ranges for the Muschelkalk sections in Fig. 12 are dashed, those from the Tethys composite shown as solid. The Olenekian-Anisian boundary interval is shown in grey based on the proposed criteria in the Dęsli Caira section (Grădinaru et al. 2007; Hounslow et al. 2007b). Radiometric ages from Muttoni et al. (2004), Brack et al. (2005) and Lehrmann et al. (2007). Palynostratigraphy zones refer to Figs. 6 and 7. Dashed zone boundaries indicate uncertain base (or top). The Spitsbergen magnetostratigraphy has been arbitrary stretched over the Anisian-Ladinian boundary interval to provide a better visual fit to the global polarity timescale.

	Dec	Inc	K	α95	Nl/Np	Reversal Test	G_O/G_C	Plat	Plong	Dp/Dm
	MES section (Vendomdalen Mb)									
Line fits	36.3	59.7	36.3	5.0	24/0	-	-	50	154	5.7/7.5
GC means^{+}	38.9	67.7	36.5	3.1	24/34	R-	15.7/6.5*	59	147	4.3/5.2
	ME section (Botneheia Fm)									
Line fits	45.3	61.9	31.3	3.7	48/0	Rc	16.9/31	50	143	4.6/6.0
GC means^{+}	39.3	71.1	25.1	2.3	48/105	Rb	8.1/8.8	64	144	3.5/4.0

Table 1. Fisher means, reversal tests and VGP poles. Nl=number of specimens using with fitted lines, and Np =number of specimens with great circle planes used in the determining the mean direction. α_{95}, Fisher 95% cone of confidence. k, Fisher precision parameter. G_O is the angular separation between the inverted reverse and normal directions, and Gc is the critical value for the reversal test. In the reversal test the Go/Gc values flagged with * indicate common K-values, others not flagged have statistically different K-values for reverse and normal populations, in which case a simulation reversal test was performed. Plat and Plong are the latitude and longitude of the mean virtual geomagnetic pole. $^{+}$=great circle combined mean.

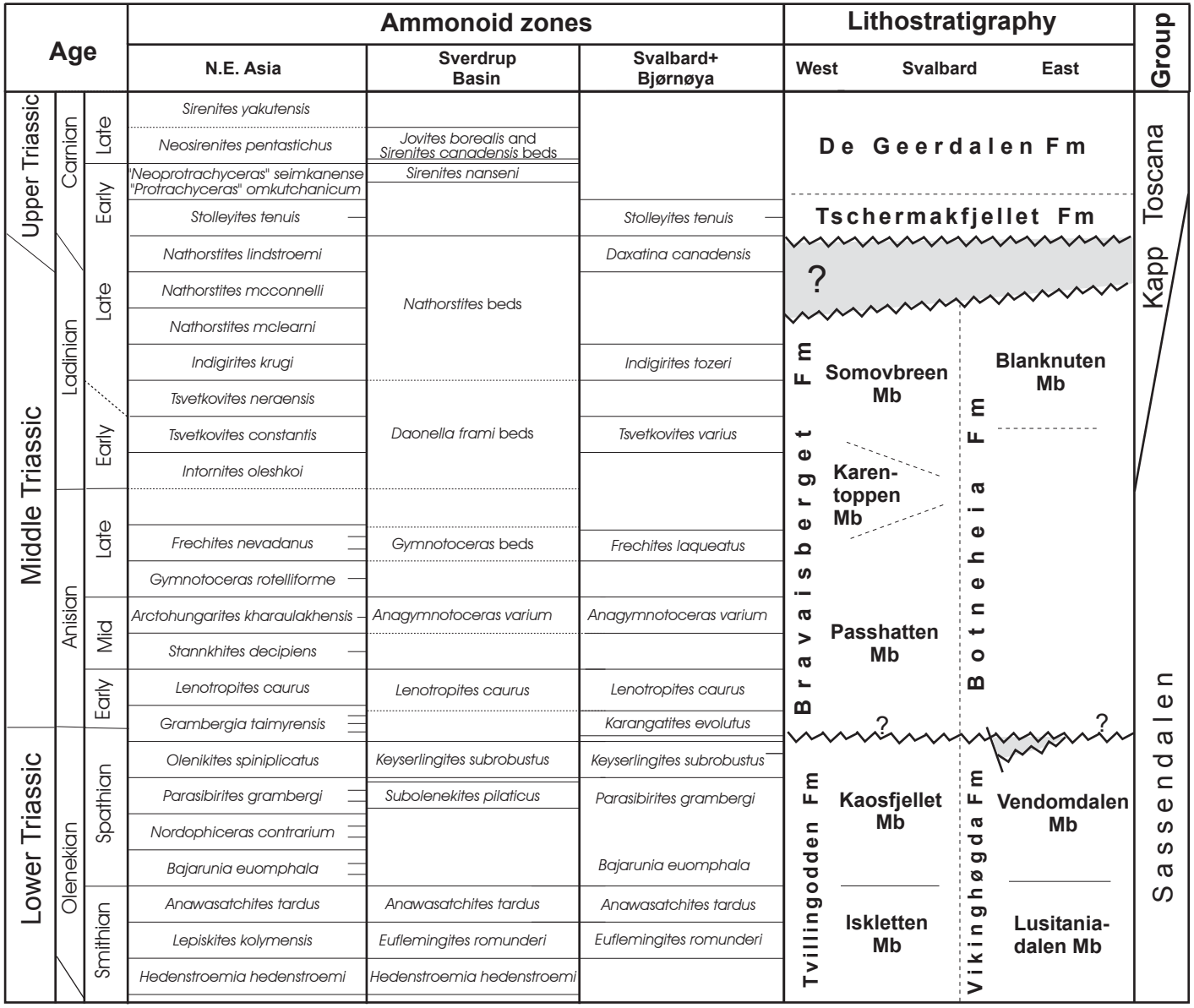
Age
Ammonoid zones
Lithostratigraphy
Group
N.E. Asia
Sverdrup Basin
Svalbard+ Bjørnøya
West
Svalbard
East
Upper Triassic
Middle Triassic
Lower Triassic
Carnian
Ladinian
Anisian
Olenekian
Smithian
Late
Early
Late
Early
Late
Mid
Early
Spathian
Sirenites yakutensis
Neosirenites pentastichus
"Neoprotrachyceras" seimkanense
"Protrachyceras" omkutchanicum
Stolleyites tenuis
Nathorstites lindstroemi
Nathorstites mcconnelli
Nathorstites mclearni
Indigirites krugi
Tsvetkovites neraensis
Tsvetkovites constantis
Intornites oleshkoi
Frechites nevadanus
Gymnotoceras rotelliforme
Arctohungarites kharaulakhensis
Stannkhites decipiens
Lenotropites caurus
Grambergia taimyrensis
Olenikites spiniplicatus
Parasibirites grambergi
Nordophiceras contrarium
Bajarunia euomphala
Anawasatchites tardus
Lepiskites kolymensis
Hedenstroemia hedenstroemi
Jovites borealis and Sirenites canadensis beds
Sirenites nanseni
Nathorstites beds
Daonella frami beds
Gymnotoceras beds
Anagymnotoceras varium
Lenotropites caurus
Keyserlingites subrobustus
Subolenekites pilaticus
Anawasatchites tardus
Euflemingites romunderi
Hedenstroemia hedenstroemi
Stolleyites tenuis
Daxatina canadensis
Indigirites tozeri
Tsvetkovites varius
Frechites laqueatus
Anagymnotoceras varium
Lenotropites caurus
Karangatites evolutus
Keyserlingites subrobustus
Parasibirites grambergi
Bajarunia euomphala
Anawasatchites tardus
Euflemingites romunderi
De Geerdalen Fm
Tschermakfjellet Fm
?
Bravaisberget Fm
Somovbreen Mb
Karen-toppen Mb
Passhatten Mb
Botneheia Fm
Blanknuten Mb
?
?
Tvillingodden Fm
Kaosfjellet Mb
Iskletten Mb
Vikinghøgda Fm
Vendomdalen Mb
Lusitania-dalen Mb
Kapp Toscana
Sassendalen

Figure 1.

Fig. 2.

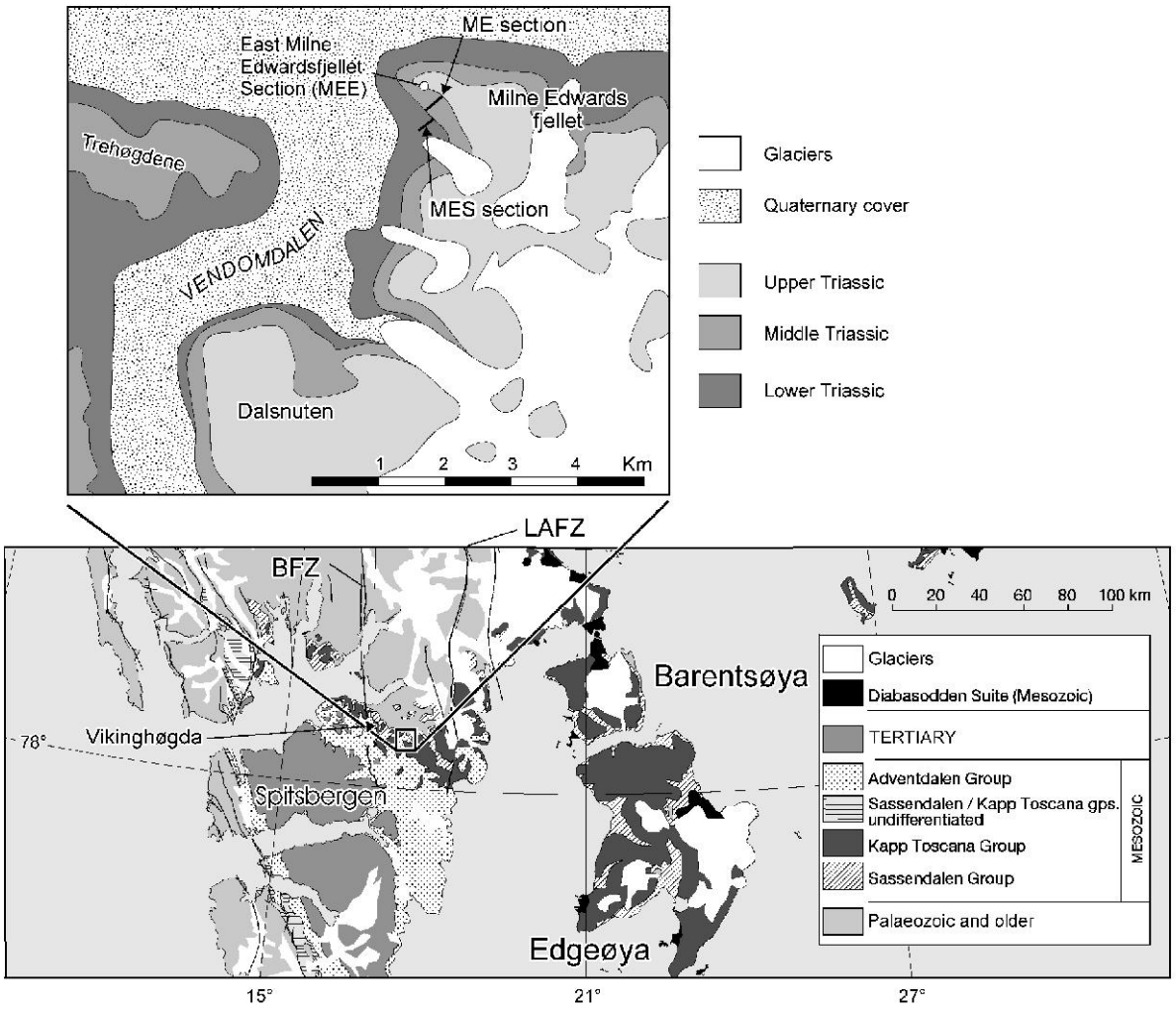
East Milne Edwardsfjellet Section (MEE)
ME section
Milne Edwards fjellet
Trehøgdene
MES section
VENDOMDALEN
Dalsnuten
1 2 3 4 Km
Glaciers
Quaternary cover
Upper Triassic
Middle Triassic
Lower Triassic
LAFZ
BFZ
Barentsøya
78°
Vikinghøgda
Spitsbergen
Edgeøya
0 20 40 60 80 100 km
Glaciers
Diabasodden Suite (Mesozoic)
TERTIARY
Adventdalen Group
Sassendalen / Kapp Toscana gps. undifferentiated
Kapp Toscana Group
Sassendalen Group
MESOZOIC
Palaeozoic and older
15°
21°
27°

Fig. 3.

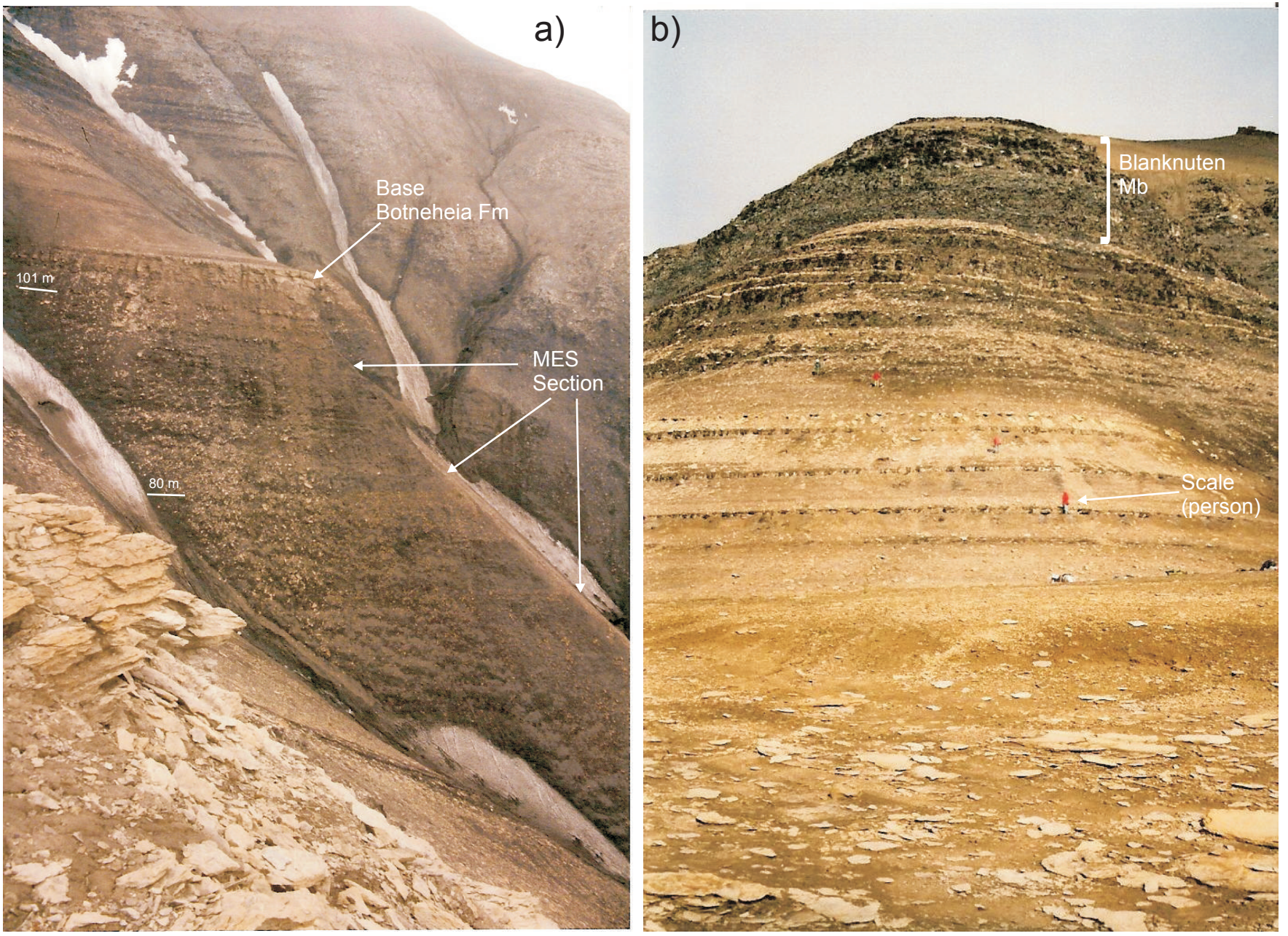
a)
Base
Botneheia Fm
101 m
MES
Section
80 m
b)
Blanknuten
Mb
Scale
(person)

Fig. 4.

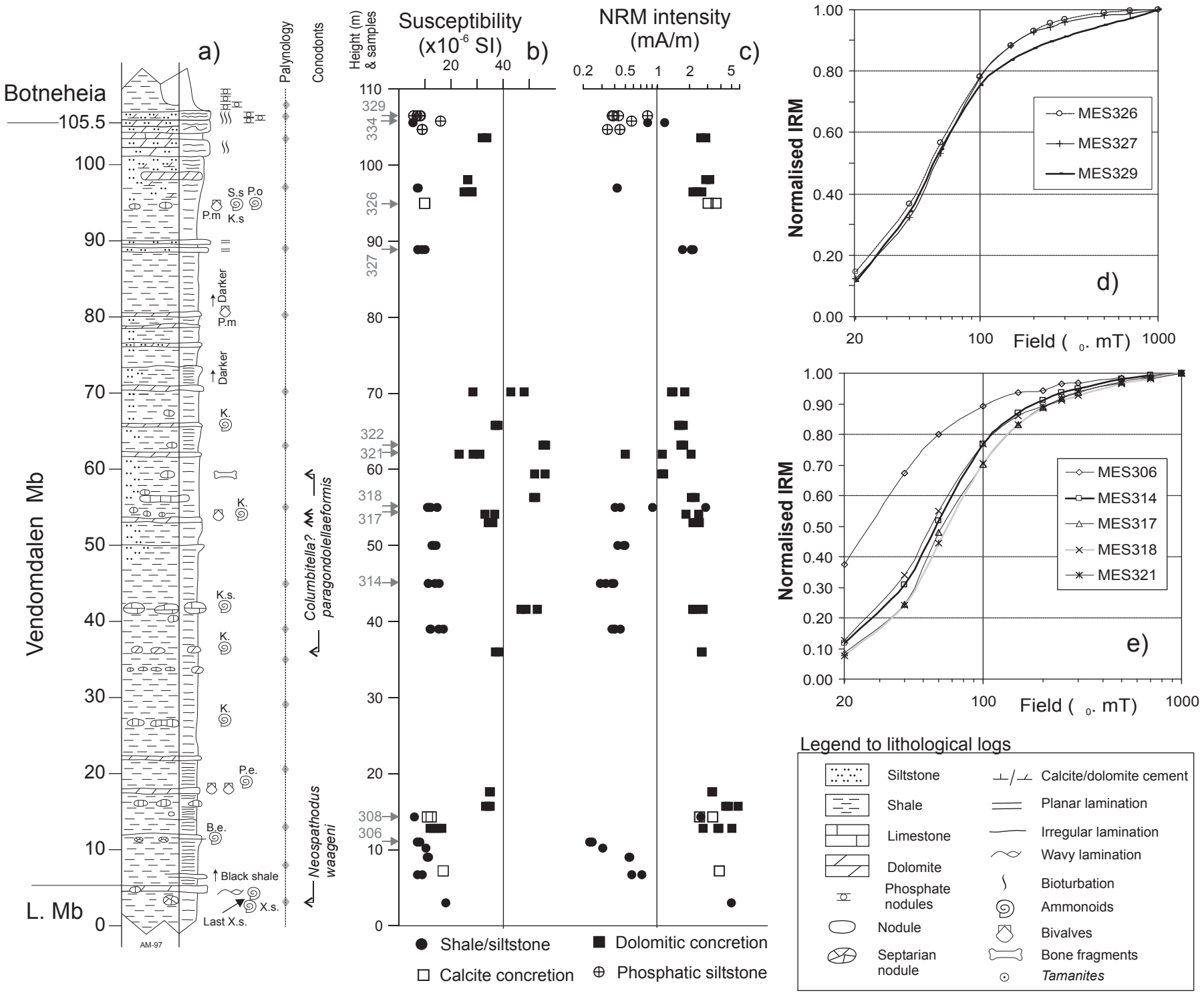
a)
Botneheia
105.5
Vendomdalen Mb
L. Mb
Palynology
Conodonts
S.s
P.o
P.m
K.s
Darker
P.m
Darker
K.
K.
K.s.
K.
K.
P.e.
B.e.
Black shale
X.s.
Last X.s.
AM-97
Columbitella? paragondolellaeformis
Neospathodus waageni
Height (m) & samples
Susceptibility (x10-6 SI)
b)
NRM intensity (mA/m)
c)
Shale/siltstone
Dolomitic concretion
Calcite concretion
Phosphatic siltstone
Normalised IRM
MES326
MES327
MES329
d)
Field (0. mT)
MES306
MES314
MES317
MES318
MES321
e)
Legend to lithological logs
Siltstone
Shale
Limestone
Dolomite
Phosphate nodules
Nodule
Septarian nodule
Calcite/dolomite cement
Planar lamination
Irregular lamination
Wavy lamination
Bioturbation
Ammonoids
Bivalves
Bone fragments
Tamanites

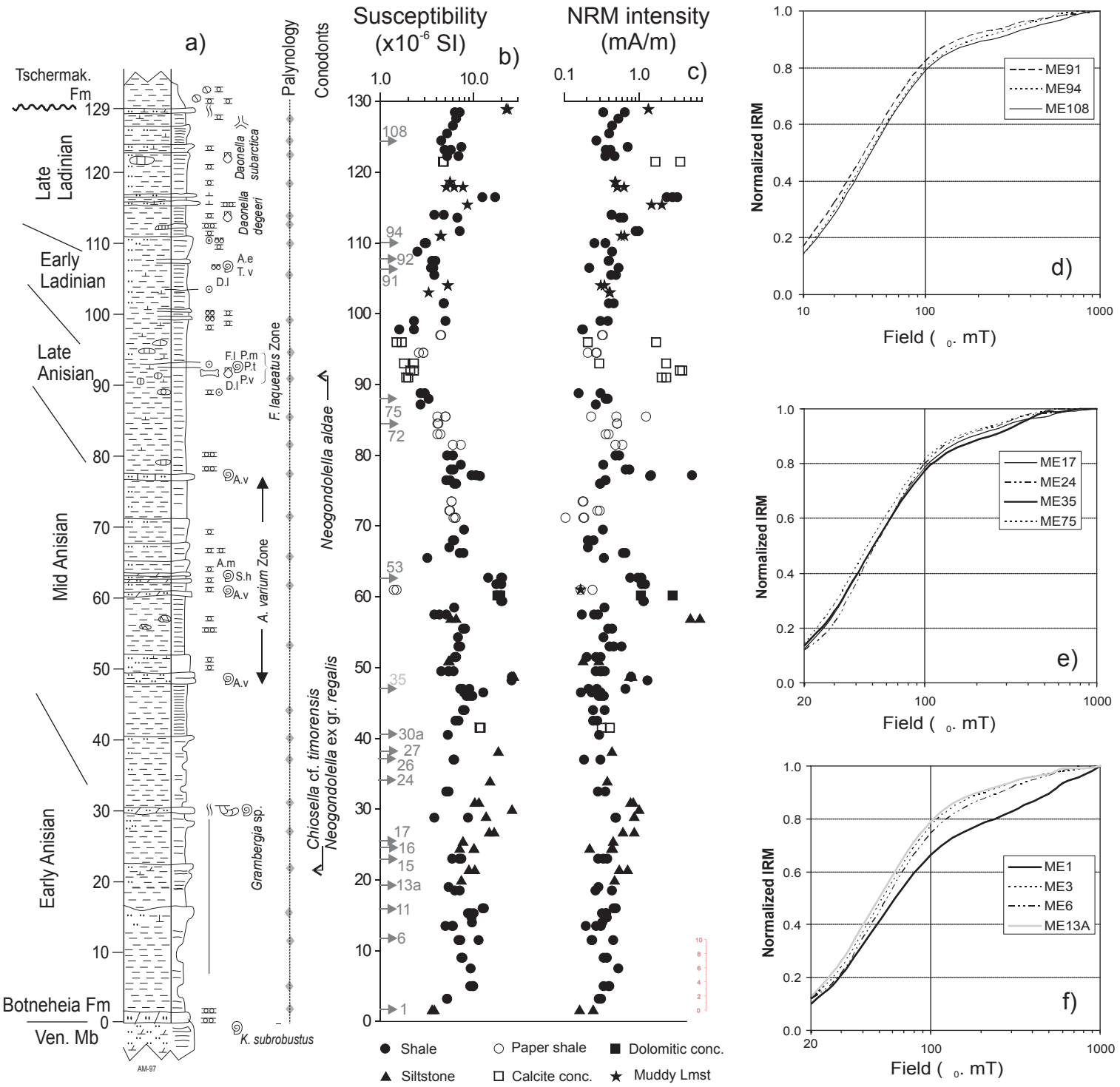
a)
Tschermak. Fm
Late Ladinian
Early Ladinian
Late Anisian
Mid Anisian
Early Anisian
Botneheia Fm
Ven. Mb
Palynology
Conodonts
Daonella subarctica
Daonella degeeri
A.e
T. v
D.I
F.l P.m
P.t
P.v
D.I
F. laqueatus Zone
A.v
A.m
S.h
A.v
A. varium Zone
A.v
Grambergia sp.
K. subrobustus
AM-97
Susceptibility (x10-6 SI)
b)
1.0
10.0
NRM intensity (mA/m)
0.1
1.0
c)
Neogondolella aldae
Chiosella cf. timorensis
Neogondolella ex gr. regalis
108
94
92
91
75
72
53
35
30a
27
26
24
17
16
15
13a
11
6
1
Shale
Paper shale
Dolomitic conc.
Siltstone
Calcite conc.
Muddy Lmst
Normalized IRM
ME91
ME94
ME108
d)
Field (0. mT)
ME17
ME24
ME35
ME75
e)
ME1
ME3
ME6
ME13A
f)

Fig. 5.

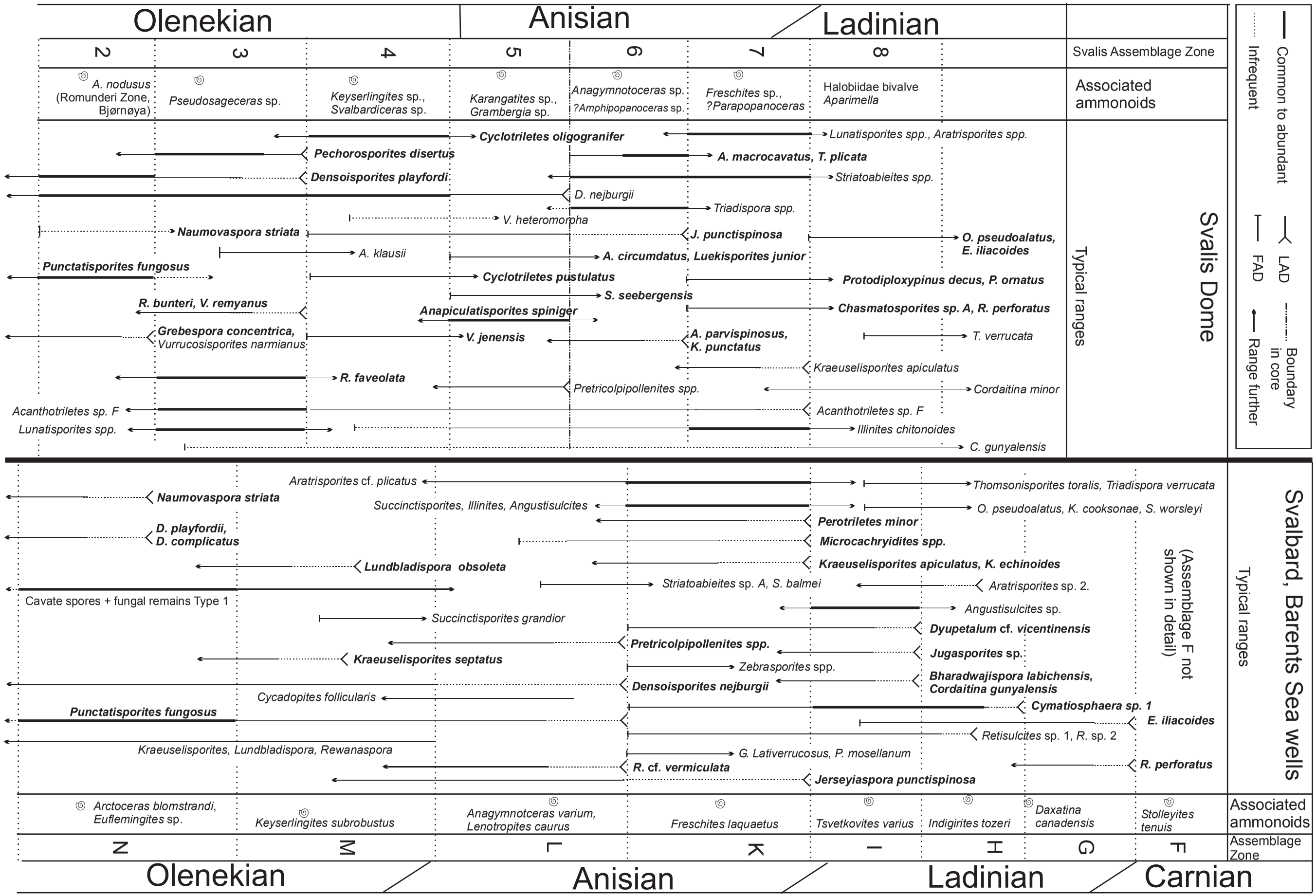
Olenekian
Anisian
Ladinian
2
3
4
5
6
7
8
Svalis Assemblage Zone
Associated ammonoids
A. nodusus (Romunderi Zone, Bjørnøya)
Pseudosageceras sp.
Keyserlingites sp., Svalbardiceras sp.
Karangatites sp., Grambergia sp.
Anagymnotoceras sp.
?Amphipopanoceras sp.
Freschites sp., ?Parapopanoceras
Halobiidae bivalve Aparimella
Cyclotriletes oligogranifer
Lunatisporites spp., Aratrisporites spp.
Pechorosporites disertus
A. macrocavatus, T. plicata
Densoisporites playfordi
Striatoabieites spp.
D. nejburgii
Triadispora spp.
V. heteromorpha
Naumovaspora striata
J. punctispinosa
O. pseudoalatus, E. iliacoides
A. klausii
A. circumdatus, Luekisporites junior
Punctatisporites fungosus
Cyclotriletes pustulatus
Protodiploxypinus decus, P. ornatus
S. seebergensis
R. bunteri, V. remyanus
Chasmatosporites sp. A, R. perforatus
Anapiculatisporites spiniger
Grebespora concentrica, Vurrucosisporites narmianus
V. jenensis
A. parvispinosus, K. punctatus
T. verrucata
Kraeuselisporites apiculatus
R. faveolata
Pretricolpipollenites spp.
Cordaitina minor
Acanthotriletes sp. F
Acanthotriletes sp. F
Lunatisporites spp.
Illinites chitonoides
C. gunyalensis
Typical ranges
Svalis Dome
Common to abundant
Infrequent
LAD
FAD
Boundary in core
Range further
Aratrisporites cf. plicatus
Thomsonisporites toralis, Triadispora verrucata
Naumovaspora striata
Succinctisporites, Illinites, Angustisulcites
O. pseudoalatus, K. cooksonae, S. worsleyi
Perotriletes minor
D. playfordii, D. complicatus
Microcachryidites spp.
Lundbladispora obsoleta
Kraeuselisporites apiculatus, K. echinoides
Striatoabieites sp. A, S. balmei
Aratrisporites sp. 2.
Cavate spores + fungal remains Type 1
Angustisulcites sp.
Succinctisporites grandior
Dyupetalum cf. vicentinensis
Pretricolpipollenites spp.
Jugasporites sp.
Kraeuselisporites septatus
Zebrasporites spp.
Bharadwajispora labichensis, Cordaitina gunyalensis
Densoisporites nejburgii
Cycadopites follicularis
Cymatiosphaera sp. 1
Punctatisporites fungosus
E. iliacoides
Retisulcites sp. 1, R. sp. 2
Kraeuselisporites, Lundbladispora, Rewanaspora
G. Lativerrucosus, P. mosellanum
R. perforatus
R. cf. vermiculata
Jerseyiaspora punctispinosa
(Assemblage F not shown in detail)
Typical ranges
Svalbard, Barents Sea wells
Arctoceras blomstrandi, Euflemingites sp.
Keyserlingites subrobustus
Anagymnotceras varium, Lenotropites caurus
Freschites laquaetus
Tsvetkovites varius
Indigirites tozeri
Daxatina canadensis
Stolleyites tenuis
Associated ammonoids
N
M
L
K
I
H
G
F
Assemblage Zone
Olenekian
Anisian
Ladinian
Carnian

Fig. 6

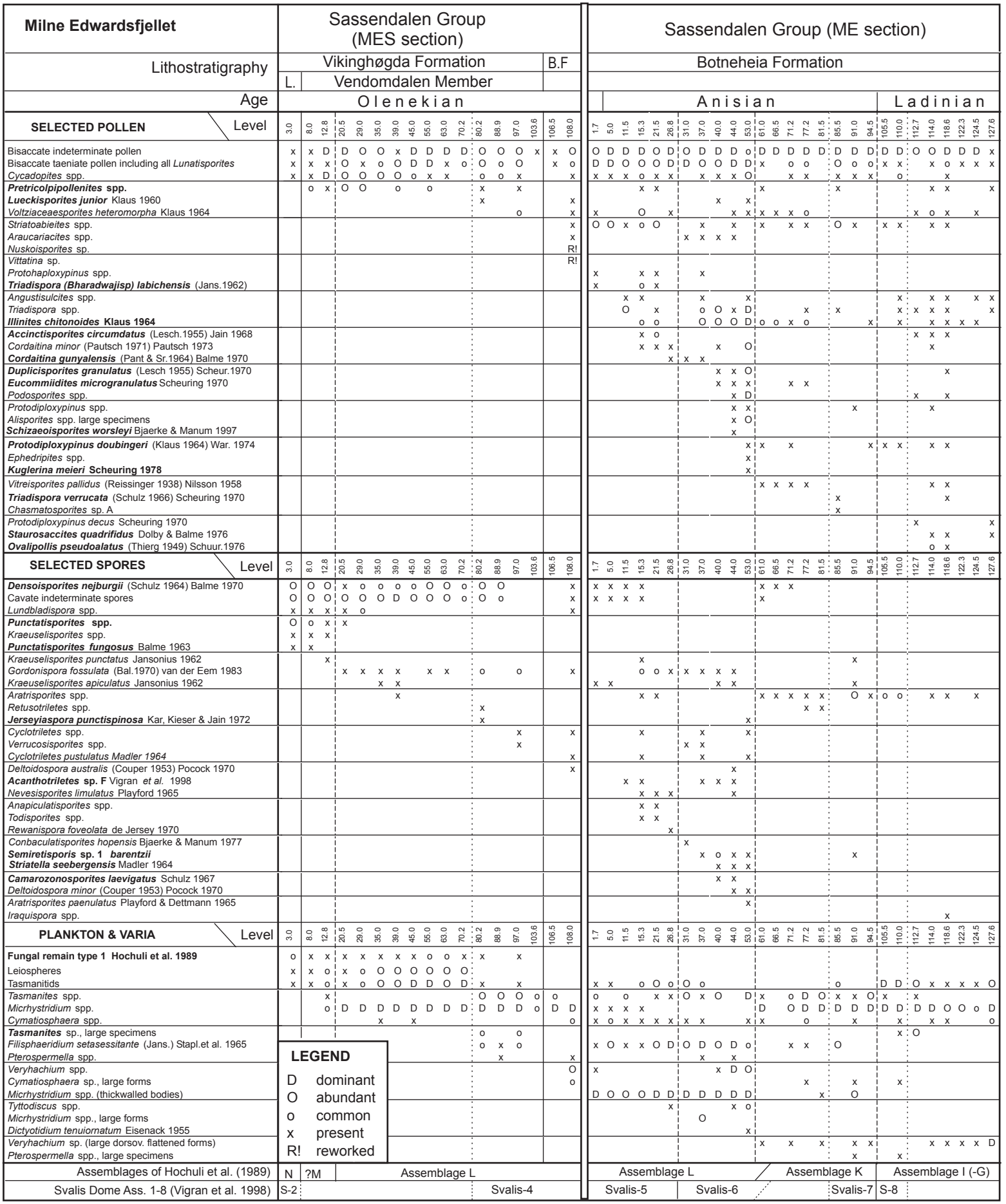
Milne Edwardsfjellet
Sassendalen Group (MES section)
Sassendalen Group (ME section)
Lithostratigraphy
Vikinghøgda Formation
B.F
L.
Vendomdalen Member
Botneheia Formation
Age
Olenekian
Anisian
Ladinian
SELECTED POLLEN
Level
SELECTED SPORES
PLANKTON & VARIA
Bisaccate indeterminate pollen
Bisaccate taeniate pollen including all Lunatisporites
Cycadopites spp.
Pretricolpipollenites spp.
Lueckisporites junior Klaus 1960
Voltziaceaesporites heteromorpha Klaus 1964
Striatoabieites spp.
Araucariacites spp.
Nuskoisporites sp.
Vittatina sp.
Protohaploxypinus spp.
Triadispora (Bharadwajisp) labichensis (Jans.1962)
Angustisulcites spp.
Triadispora spp.
Illinites chitonoides Klaus 1964
Accinctisporites circumdatus (Lesch.1955) Jain 1968
Cordaitina minor (Pautsch 1971) Pautsch 1973
Cordaitina gunyalensis (Pant & Sr.1964) Balme 1970
Duplicisporites granulatus (Lesch 1955) Scheur.1970
Eucommiidites microgranulatus Scheuring 1970
Podosporites spp.
Protodiploxypinus spp.
Alisporites spp. large specimens
Schizaeoisporites worsleyi Bjaerke & Manum 1997
Protodiploxypinus doubingeri (Klaus 1964) War. 1974
Ephedripites spp.
Kuglerina meieri Scheuring 1978
Vitreisporites pallidus (Reissinger 1938) Nilsson 1958
Triadispora verrucata (Schulz 1966) Scheuring 1970
Chasmatosporites sp. A
Protodiploxypinus decus Scheuring 1970
Staurosaccites quadrifidus Dolby & Balme 1976
Ovalipollis pseudoalatus (Thierg 1949) Schuur.1976
Densoisporites nejburgii (Schulz 1964) Balme 1970
Cavate indeterminate spores
Lundbladispora spp.
Punctatisporites spp.
Kraeuselisporites spp.
Punctatisporites fungosus Balme 1963
Kraeuselisporites punctatus Jansonius 1962
Gordonispora fossulata (Bal.1970) van der Eem 1983
Kraeuselisporites apiculatus Jansonius 1962
Aratrisporites spp.
Retusotriletes spp.
Jerseyiaspora punctispinosa Kar, Kieser & Jain 1972
Cyclotriletes spp.
Verrucosisporites spp.
Cyclotriletes pustulatus Madler 1964
Deltoidospora australis (Couper 1953) Pocock 1970
Acanthotriletes sp. F Vigran et al. 1998
Nevesisporites limulatus Playford 1965
Anapiculatisporites spp.
Todisporites spp.
Rewanispora foveolata de Jersey 1970
Conbaculatisporites hopensis Bjaerke & Manum 1977
Semiretisporis sp. 1 barentzii
Striatella seebergensis Madler 1964
Camarozonosporites laevigatus Schulz 1967
Deltoidospora minor (Couper 1953) Pocock 1970
Aratrisporites paenulatus Playford & Dettmann 1965
Iraquispora spp.
Fungal remain type 1 Hochuli et al. 1989
Leiospheres
Tasmanitids
Tasmanites spp.
Micrhystridium spp.
Cymatiosphaera spp.
Tasmanites sp., large specimens
Filisphaeridium setasessitante (Jans.) Stapl.et al. 1965
Pterospermella spp.
Veryhachium spp.
Cymatiosphaera sp., large forms
Micrhystridium spp. (thickwalled bodies)
Tyttodiscus spp.
Micrhystridium spp., large forms
Dictyotidium tenuiornatum Eisenack 1955
Veryhachium sp. (large dorsov. flattened forms)
Pterospermella spp., large specimens
LEGEND
D dominant
O abundant
o common
x present
R! reworked
Assemblages of Hochuli et al. (1989)
N
?M
Assemblage L
Assemblage L
Assemblage K
Assemblage I (-G)
Svalis Dome Ass. 1-8 (Vigran et al. 1998)
S-2
Svalis-4
Svalis-5
Svalis-6
Svalis-7
S-8

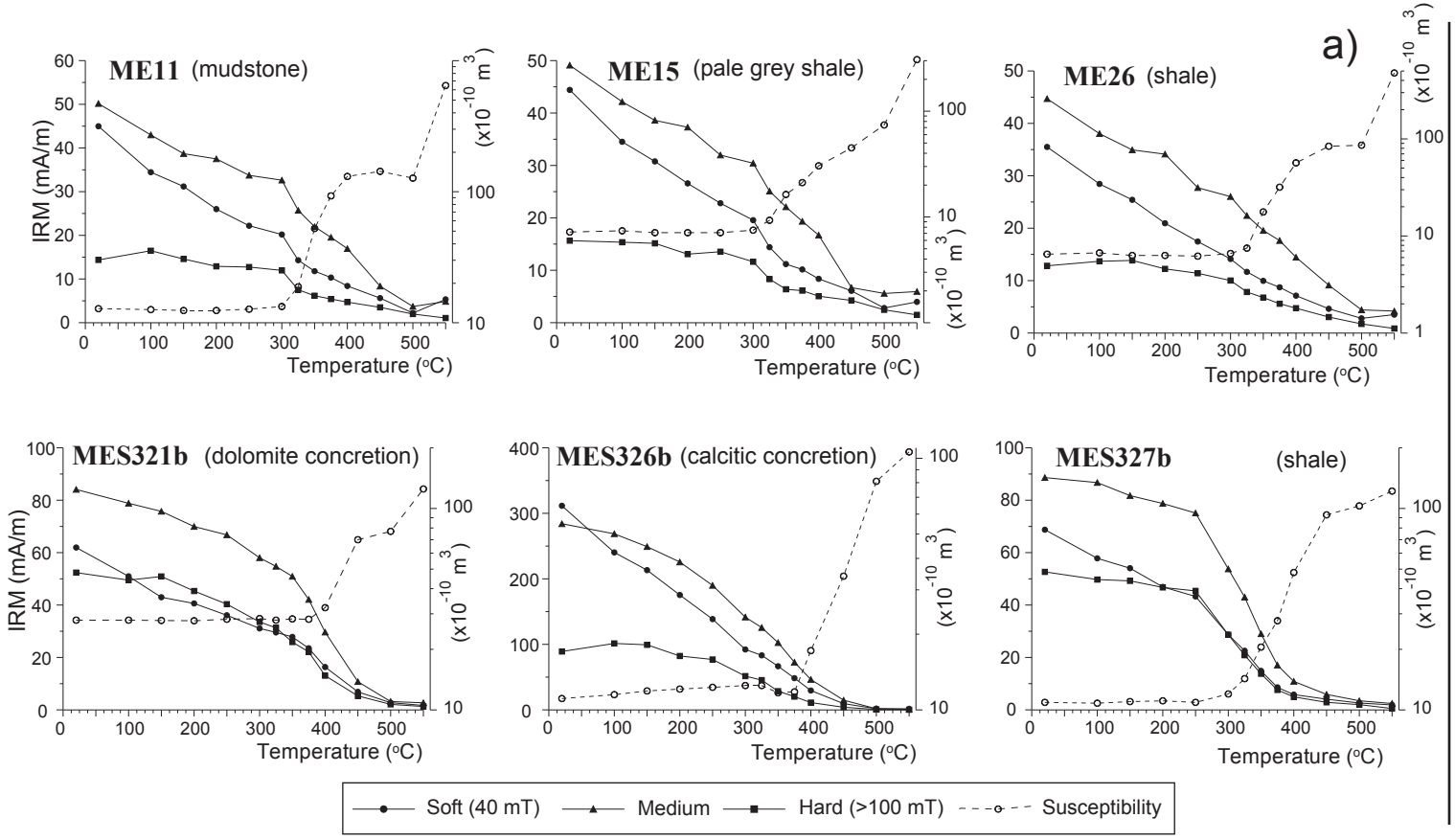
a)
ME11 (mudstone)
ME15 (pale grey shale)
ME26 (shale)
MES321b (dolomite concretion)
MES326b (calcitic concretion)
MES327b (shale)
IRM (mA/m)
(x10^-10 m^3)
Temperature (°C)
Soft (40 mT)
Medium
Hard (>100 mT)
Susceptibility

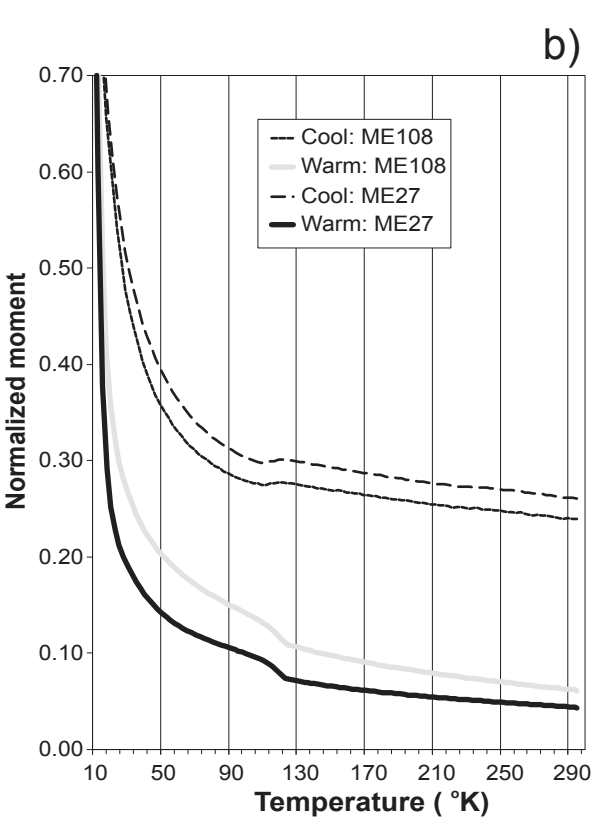
b)
Cool: ME108
Warm: ME108
Cool: ME27
Warm: ME27
Normalized moment
Temperature (°K)

Fig. 8.

Fig. 9

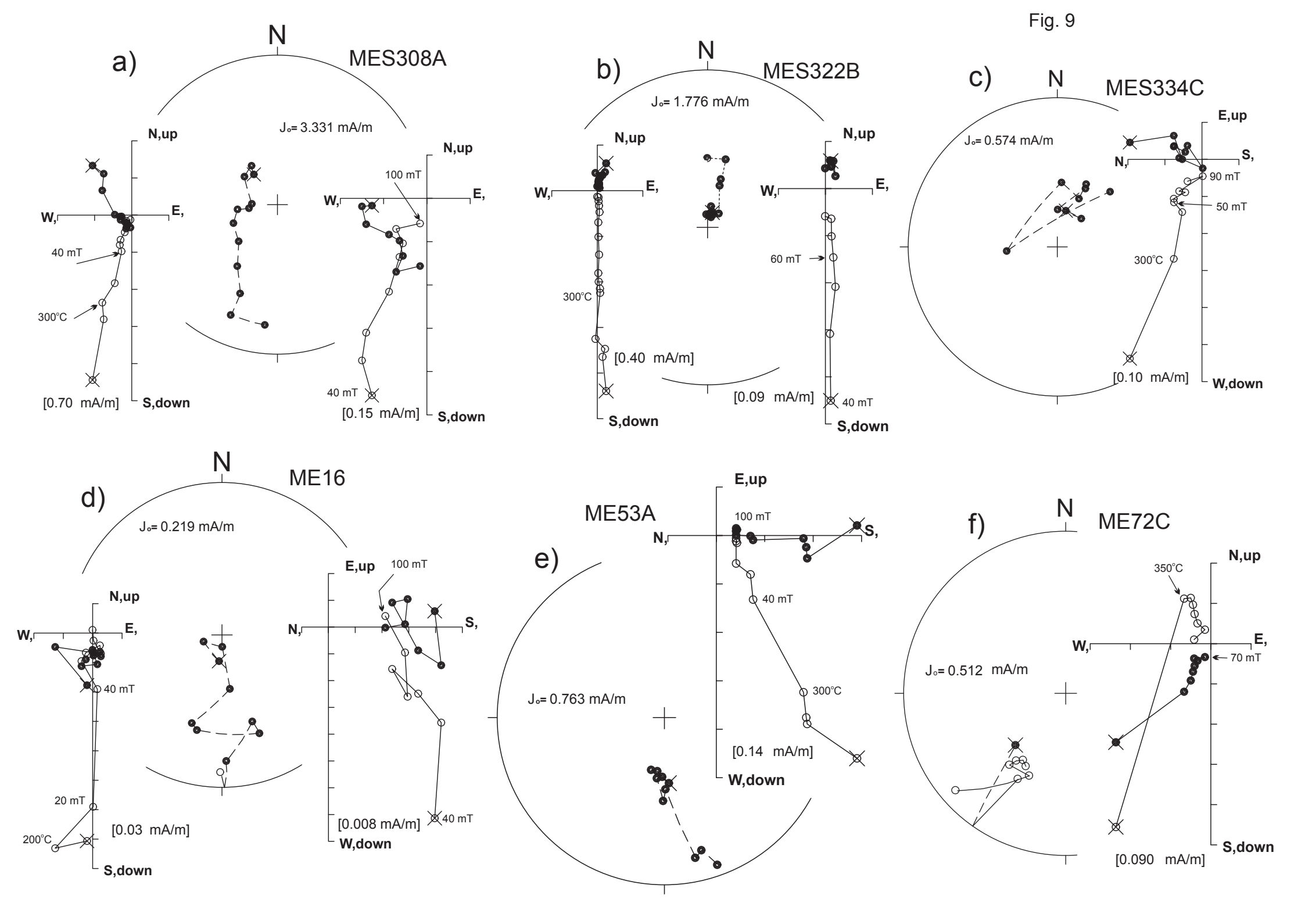
a)
MES308A
N
Jₒ= 3.331 mA/m
N,up
W,
E,
40 mT
300°C
[0.70 mA/m]
S,down
100 mT
[0.15 mA/m]
b)
MES322B
Jₒ= 1.776 mA/m
[0.40 mA/m]
60 mT
[0.09 mA/m]
c)
MES334C
Jₒ= 0.574 mA/m
E,up
N,
S,
90 mT
50 mT
300°C
[0.10 mA/m]
W,down
d)
ME16
Jₒ= 0.219 mA/m
20 mT
200°C
[0.03 mA/m]
[0.008 mA/m]
e)
ME53A
Jₒ= 0.763 mA/m
[0.14 mA/m]
f)
ME72C
350°C
70 mT
[0.090 mA/m]

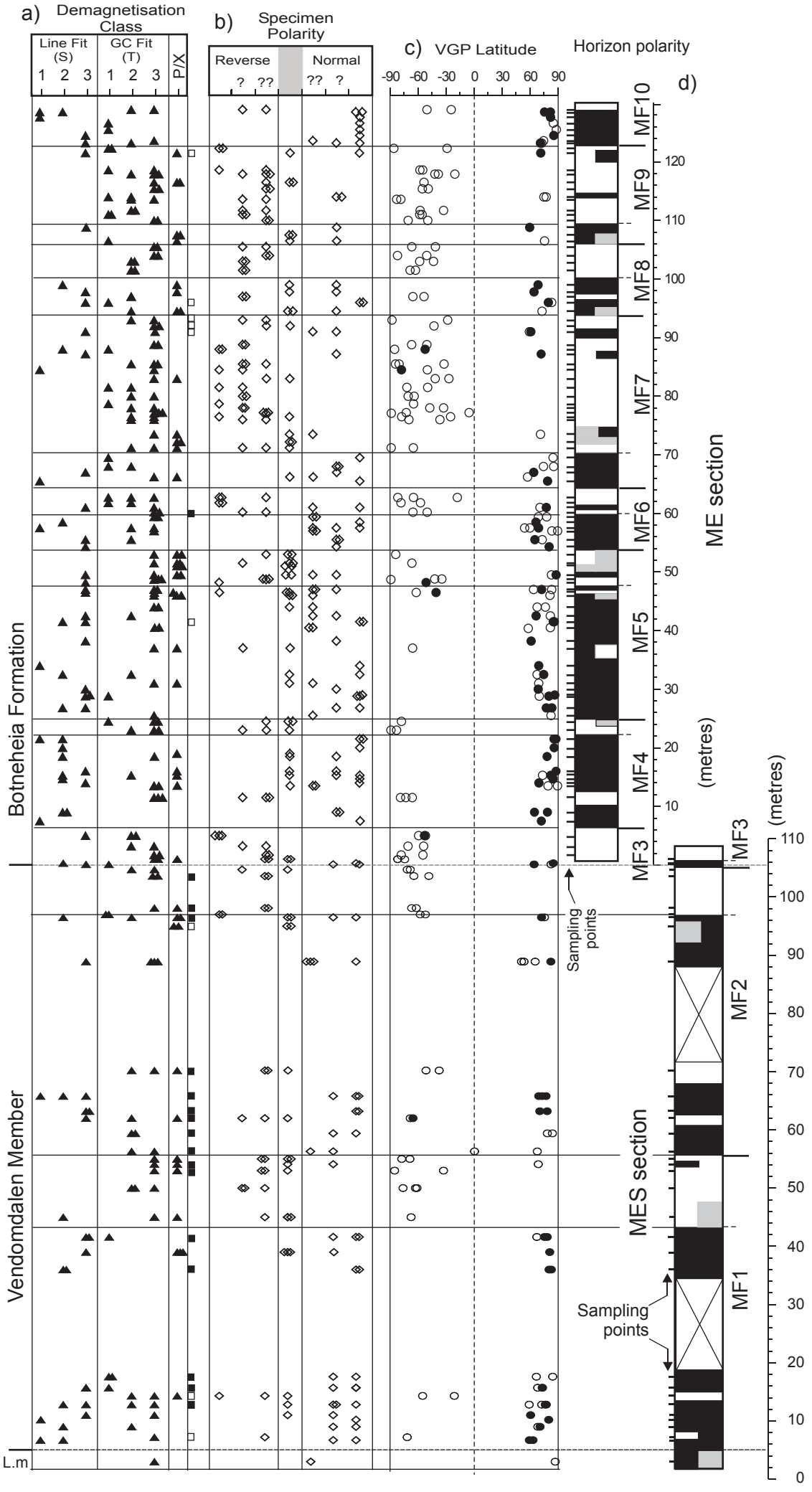
a) Demagnetisation Class
Line Fit (S)
GC Fit (T)
1 2 3 1 2 3 P/X
b) Specimen Polarity
Reverse
Normal
? ?? ?? ?
c) VGP Latitude
-90 -60 -30 0 30 60 90
Horizon polarity
d)
MF10
MF9
MF8
MF7
MF6
MF5
MF4
MF3
ME section
(metres)
Botneheia Formation
Vendomdalen Member
Sampling points
MF3
MF2
MF1
MES section
(metres)
L.m

Fig. 10.

Fig. 11.

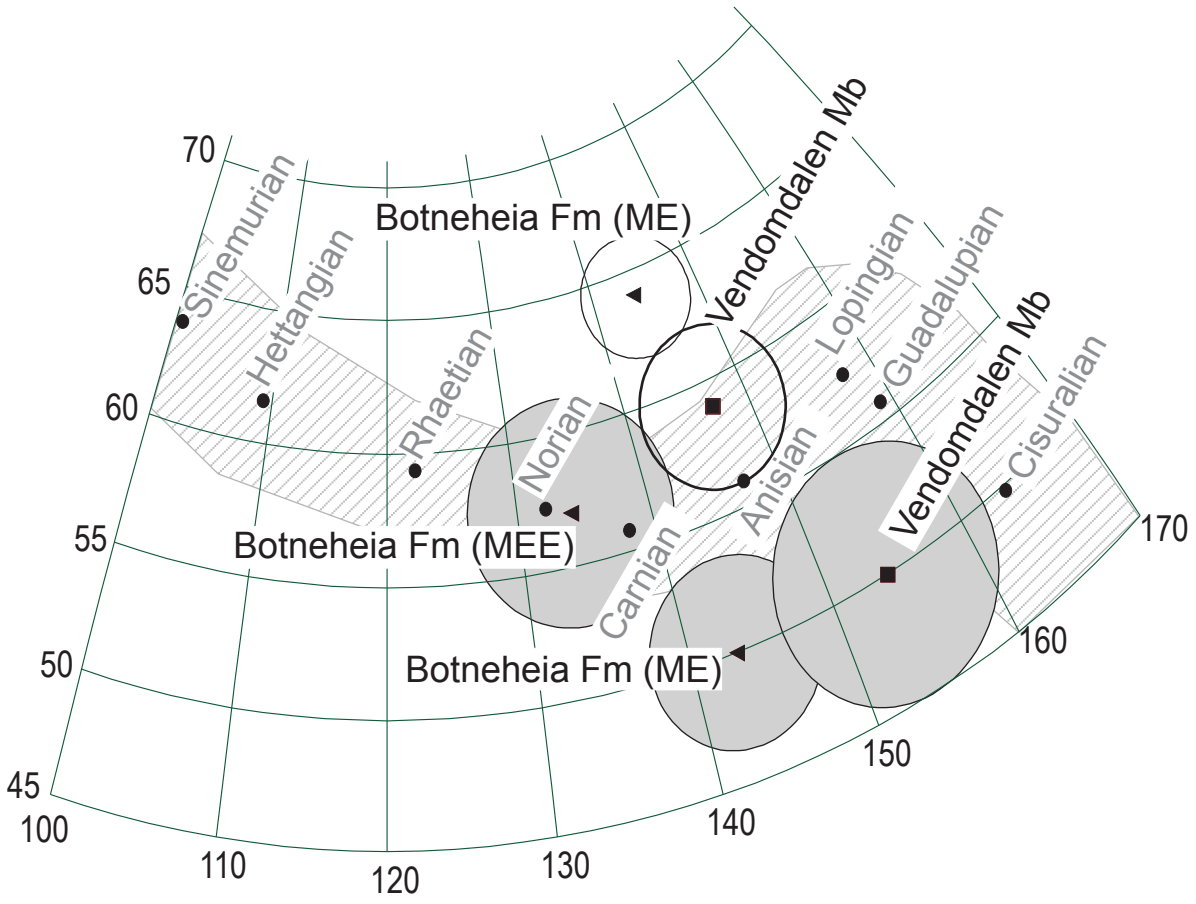
70
65
60
55
50
45
100
110
120
130
140
150
160
170
Sinemurian
Hettangian
Rhaetian
Norian
Carnian
Anisian
Lopingian
Guadalupian
Cisuralian
Botneheia Fm (ME)
Botneheia Fm (MEE)
Botneheia Fm (ME)
Vendomdalen Mb
Vendomdalen Mb

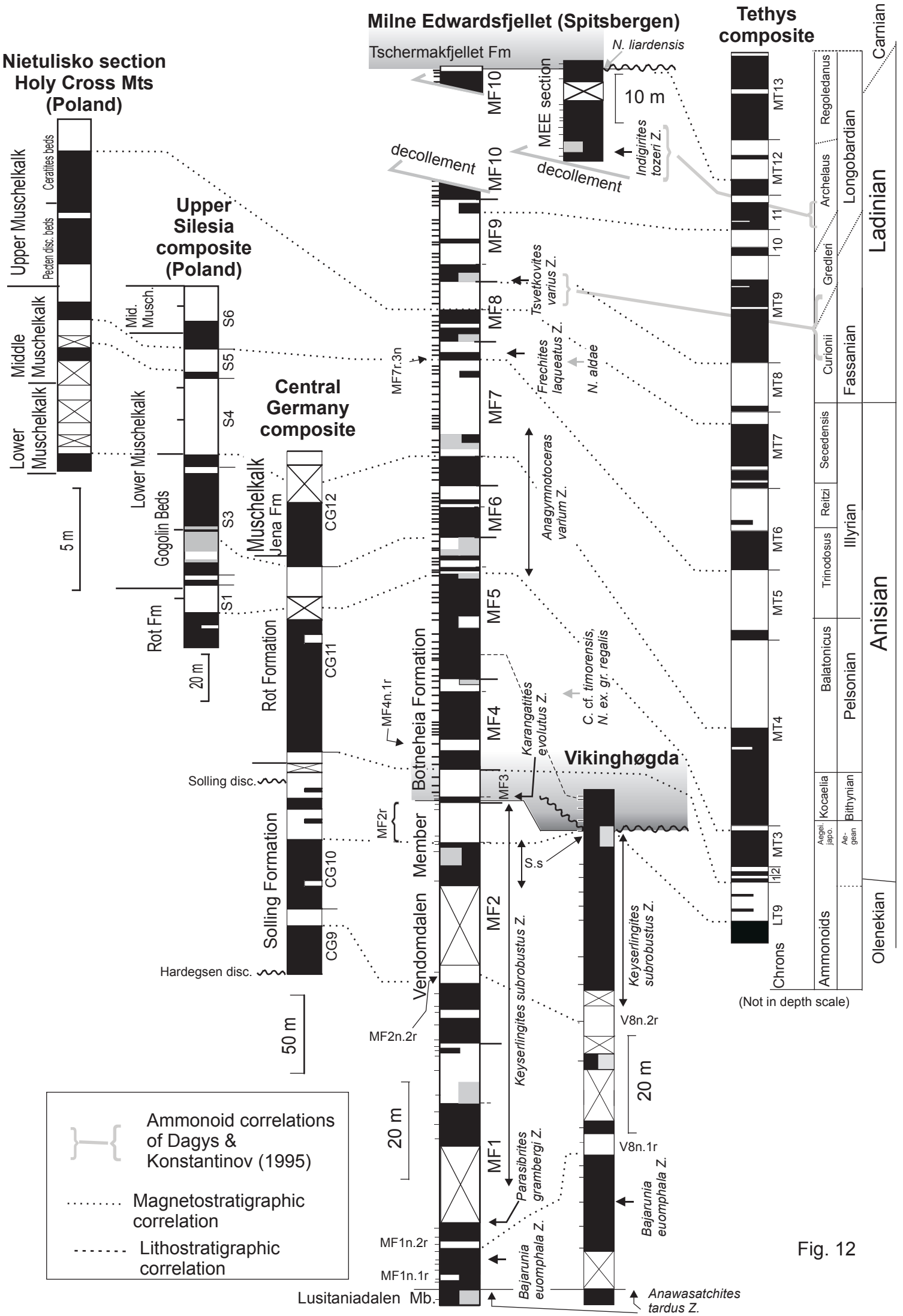
Nietulisko section
Holy Cross Mts
(Poland)
Upper Muschelkalk
Ceratites beds
Pecten disc. beds
Middle Muschelkalk
Lower Muschelkalk
5 m
Upper Silesia composite (Poland)
Mid. Musch.
S6
S5
S4
S3
S1
Lower Muschelkalk
Gogolin Beds
Rot Fm
20 m
Central Germany composite
Muschelkalk
Jena Fm
CG12
CG11
CG10
CG9
Rot Formation
Solling Formation
Solling disc.
Hardegsen disc.
50 m
Milne Edwardsfjellet (Spitsbergen)
Tschermakfjellet Fm
N. liardensis
MEE section
10 m
Indigirites tozeri Z.
decollement
decollement
MF10
MF9
MF8
MF7
MF6
MF5
MF4
MF3
MF2
MF1
Tsvetkovites varius Z.
Frechites laqueatus Z.
N. aldae
MF7r.3n
Anagymnotoceras varium Z.
C. cf. timorensis,
N. ex. gr. regalis
MF4n.1r
Karangatites evolutus Z.
Botneheia Formation
Vikinghøgda
MF2r
S.s
Vendomdalen Member
Keyserlingites subrobustus Z.
MF2n.2r
Keyserlingites subrobustus Z.
V8n.2r
20 m
V8n.1r
Bajarunia euomphala Z.
Parasibrites grambergi Z.
MF1n.2r
MF1n.1r
Bajarunia euomphala Z.
Lusitaniadalen Mb.
Anawasatchites tardus Z.
20 m
Tethys composite
MT13
MT12
11
10
MT9
MT8
MT7
MT6
MT5
MT4
MT3
12
LT9
Chrons
(Not in depth scale)
Regoledanus
Archelaus
Gredleri
Curionii
Secedensis
Reitzi
Trinodosus
Balatonicus
Kocaelia
Bithynian
Aegei japo.
Ae-gean
Ammonoids
Carnian
Ladinian
Anisian
Olenekian
Longobardian
Fassanian
Illyrian
Pelsonian
Ammonoid correlations of Dagys & Konstantinov (1995)
Magnetostratigraphic correlation
Lithostratigraphic correlation

Fig. 12

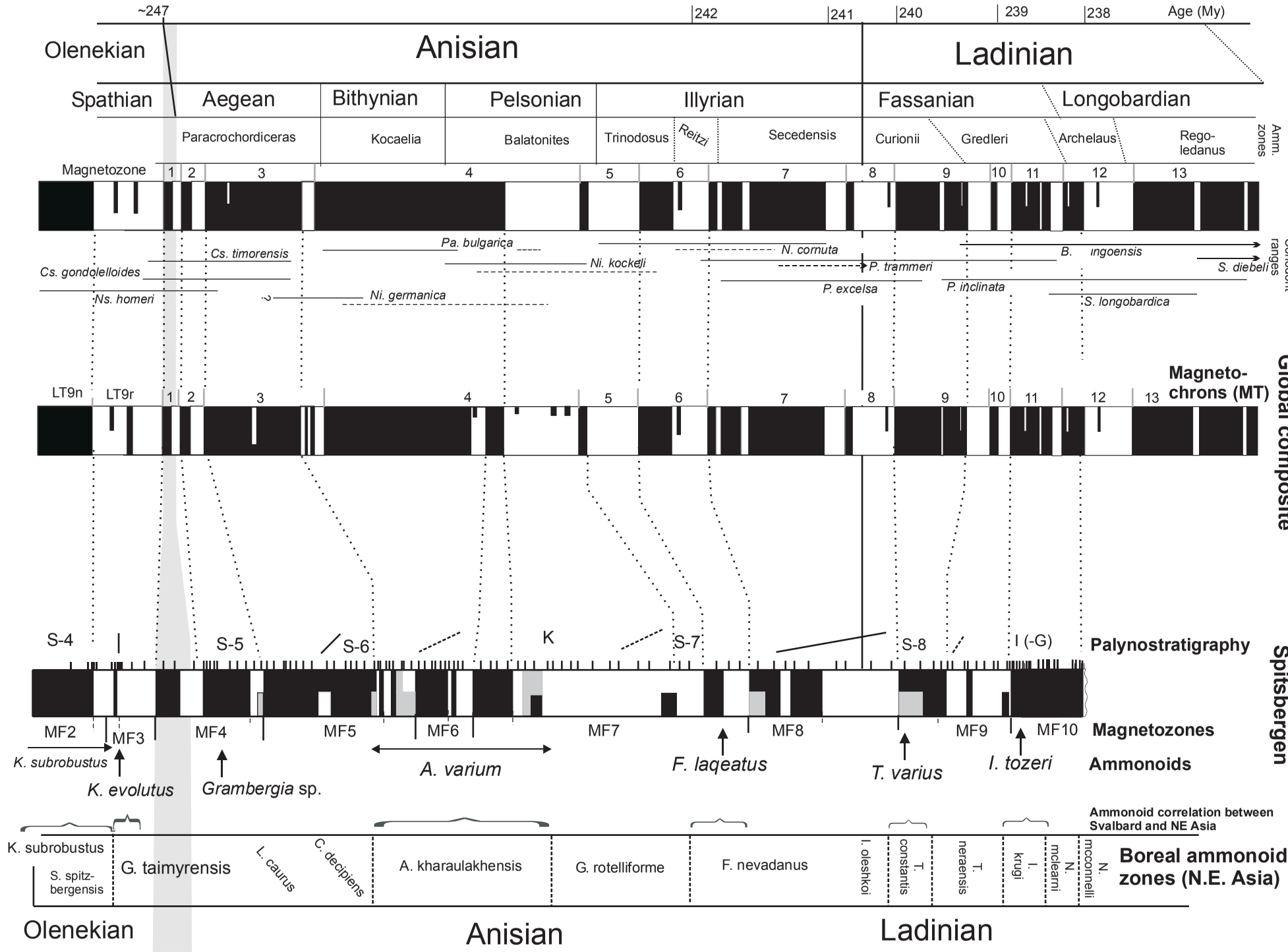
~247
242
241
240
239
238
Age (My)
Olenekian
Anisian
Ladinian
Spathian
Aegean
Bithynian
Pelsonian
Illyrian
Fassanian
Longobardian
Paracrochordiceras
Kocaelia
Balatonites
Trinodosus
Reitzi
Secedensis
Curionii
Gredleri
Archelaus
Rego-ledanus
Amm. zones
Tethys stratigraphy
Magnetozone
1
2
3
4
5
6
7
8
9
10
11
12
13
Pa. bulgarica
N. cornuta
B. ingoensis
Cs. timorensis
Ni. kockeli
P. trammeri
S. diebeli
Cs. gondolelloides
P. excelsa
P. inclinata
Ns. homeri
Ni. germanica
S. longobardica
Conodont ranges
LT9n
LT9r
Magneto-chrons (MT)
Global composite
S-4
S-5
S-6
K
S-7
S-8
I (-G)
Palynostratigraphy
Spitsbergen
MF2
MF3
MF4
MF5
MF6
MF7
MF8
MF9
MF10
Magnetozones
K. subrobustus
K. evolutus
Grambergia sp.
A. varium
F. laqeatus
T. varius
I. tozeri
Ammonoids
Ammonoid correlation between Svalbard and NE Asia
K. subrobustus
S. spitz-bergensis
G. taimyrensis
L. caurus
C. decipiens
A. kharaulakhensis
G. rotelliforme
F. nevadanus
I. oleshkoi
T. constantis
T. neraensis
I. krugi
N. mclearni
N. mconnelli
Boreal ammonoid zones (N.E. Asia)
Olenekian
Anisian
Ladinian

Fig. 13